Interpolated Variational Transition-State Theory by Mapping

José C. Corchado,[†,‡] E. Laura Coitiño,[†] Yao-Yuan Chuang,[†] Patton L. Fast,[†] and Donald G. Truhlar*[,†]

Department of Chemistry and Supercomputer Institute, University of Minnesota, Minneapolis, Minnesota 55455-0431 and Departamento de Química Física, Universidad de Extremadura, 06071 Badajoz, Spain

Received: November 7, 1997; In Final Form: January 28, 1998

We present a new systematic set of algorithms for interpolated variational transition-state theory by mapping (IVTST-M). In this method, which is designed to allow efficient direct dynamics calculations, rate constants for chemical reactions are evaluated by variational transition-state theory with multidimensional tunneling approximations based on reaction-path data. The data (energies, energy gradients, and Hessians) are computed at a small number of points along a reaction path and fitted to splines under tension as functions of a mapped independent variable that is a nonlinear function of the reaction coordinate. The theory is illustrated and tested by several examples, and standard choices are employed for all parameters and functional forms to provide a realistic test of how the method might perform when applied as an automatic scheme without fine-tuning each reaction. For eight test cases, we obtain reasonable accuracy (as compared to calculations with the same potential surface with the reaction path followed as far as necessary for convergence) with Hessians at only six nonstationary points.

1. Introduction

The goal of interfacing electronic structure theory with dynamics for the prediction of absolute reaction rates is as old as transition-state theory, probably older. To achieve this goal, several impediments must be overcome:

(1) We need to develop better methods of electronic structure theory, whether undilutedly ab initio or involving scaling, extrapolation, semiempirical elements, or density functional theory, for predicting relative energies along reaction paths.

(2) We need to develop practical, robust, and reliable dynamics methods that require a minimum of potential energy surface input.

(3) As we continue to make progress in the first two areas, we need to develop convenient, reliable algorithms that maximize the benefit-to-cost ratio for our current as yet imperfect electronic structure methods and our best available dynamics methods for rate calculations.

The present contribution is concerned with (3). Our goal is to develop methods for carrying out a variational transition-state theory calculation with multidimensional tunneling (VTST/MT) based on a minimal amount of high-level electronic structure data. In particular, we are concerned with efficient methods for direct dynamics calculations, in which the dynamical computation is based directly on the electronic structure without the intermediacy of a potential energy function. Background for VTST/MT methods[1−8] and their interface[6,7,9−19] with electronic structure theory is presented elsewhere.

2. Background

2.1. Theory. VTST/MT methods are examples of reaction-path and reaction-swath methods in which information about the potential surface is required only in a narrow valley[1−19] centered on the minimum-energy reaction path or in a somewhat wider swath[3−5,7,9,12,14,15,19] that includes broad corner-cutting regions associated with large-curvature segments of the reaction path. The algorithms considered in the present paper are restricted to reaction-path methods, in particular canonical variational theory[1−5] (CVT), improved CVT[1,3−5] (ICVT) with zero-curvature tunneling[1−5,20] (ZCT), and small-curvature tunneling[2−6,9,12] (SCT), which are explained further below, although they could be combined with reaction-swath methods in later work. A recent summary[21] of comparisons of VTST/MT methods to accurate quantal calculations indicates that reaction-path VTST/MT calculations can provide considerably greater accuracy than conventional transition-state theory over a broad range of systems. Table 1 presents a summary of some of the findings of that survey for reactions involving the transfer of protium or deuterium atoms. The harmonic CVT, CVT/ZCT, and CVT/SCT rows are particularly relevant because these are the methods that will be considered in the present paper. Table 1 shows that all three of these methods provide considerably more accurate results than conventional TST. In most cases the errors can be reduced by using microcanonical optimized multidimensional tunneling (μOMT) or including anharmonicity, but these refinements are beyond the scope of the present paper because they require more information about potential energy surfaces than is assumed to be available here. In particular, μOMT calculations require information about the potential in the reaction swath, and anharmonic calculations require cubic and quartic force constants along the reaction path, whereas the present study assumes only quadratic force constants are available.

In summary, although greater accuracy is possible when more information is available, the goal of the present study is to calculate accurate CVT, CVT/ZCT, and CVT/SCT rate constants as efficiently as possible, in particular by minimizing the number of energies, energy gradients, and Hessian matrixes that are required to be calculated by electronic structure methods. (Note: the force constants are equal to one-half times the

[†] University of Minnesota.
[‡] Universidad de Extremadura.

S1089-5639(98)00126-1 CCC: $15.00
Published on Web 03/17/1998

TABLE 1: Average Errors for VTST/MT Rate Constants for H-Atom and D-Atom Transfer Reactions Determined by Comparison to Accurate Quantal Ones for the Same Potential Energy Surface

	250 K	300 K	2400 K
no. of cases[a]	33	40	9
Average Errors (Curvilinear Harmonic)[b]			
conventional TST	630	400	190
CVT	265	174	26
ICVT	265	174	23
CVT/ZCT	151	110	25
ICVT/ZCT	151	110	23
CVT/SCT	69	55	25
ICVT/SCT	69	55	23
CVT/μOMT	41	36	31
ICVT/μOMT	41	36	29
Average Errors (Anharmonic)[b]			
ICVT/SCT	39	33	25
ICVT/μOMT	29	25	27

[a] Includes 28 collinear and 12 three-dimensional atom−diatom reactions at 300 K. For the other two temperatures, the averages are based on the subset of these cases for which data is available. [b] The value quoted is the geometric mean of the logarithmically average percentage error (LAPE) and the mean percentage error (MPE), as explained in detail in ref 21.

elements of the Hessian matrix.[22]) Since gradients are used for calculating the reaction path itself, one goal of our work will be to minimize the length of the path segment that must actually be calculated. A second goal will be to minimize the number of points along this segment at which Hessians are calculated. The approach used to attain these goals is interpolation of reaction-path properties as functions of a mapped independent variable. Thus, the algorithm is called IVTST-M, which denotes interpolated variational transition state theory (including tunneling) by mapping.

The traditional approach to converging reaction-path calculations involves calculating enough electronic structure data to converge the calculations with respect to the range of the reaction path considered and the density of points within this range. In this paradigm the dynamics algorithm is the master and the electronic structure program is the slave, of whom much is asked. However, in practical situations there is great merit in turning the master/slave relationship upside down. The electronic structure program rests after its budgeted effort, which produces a small number of energies and energy gradients on a reaction path, with at least some of these being accompanied by Hessians. The master structure-and-energy generator then requests the slave dynamics algorithm to do the best it can with the data available. Our goal here is to develop a standardized response for the slave. We envision that over the long haul one can devise better procedures than those presented here (e.g., by recognizing the relationship of reaction-path curvature to changes in internal coordinates), but the procedures presented here can fill the gap in the meantime, and furthermore our goal is to provide a baseline strategy in which one makes only conservative interpolations so that any further attempts to contribute to this problem will have a standard against which to measure themselves.

Variational transition-state theory and the numerical methods we employ for it are explained elsewhere,[1−8] and in the present study we shall concentrate on three standard dynamical levels. The first, canonical variational theory (CVT) optimizes the location of the dynamical bottleneck but neglects tunneling. The next two, CVT with zero-curvature tunneling (CVT/ZCT) and CVT with small-curvature tunneling (CVT/SCT), are based entirely on information calculated along a reaction path. In a few cases, we upgrade CVT to improved CVT (ICVT[1,3−5]). Although recent work is encouraging for our eventual ability to base such calculations on a variety of reaction-path types,[23] the present article is restricted to the tried and true choice, namely the steepest descent path in isoinertial coordinates.[20,24−26] (This path is usually called the minimum-energy path (MEP)[1,20] or intrinsic reaction path;[25] we use the former notation.) Distance along the MEP is denoted s, and F denotes the number of internal degrees of freedom (for systems with nonlinear geometries on the reaction path, $F = 3N - 6$, where N is the number of atoms).

A CVT/ZCT calculation with harmonic treatment of vibrations requires the following information along the reaction path: (i) the potential energy, $V_{MEP}(s)$; (ii) the frequencies, $\{\omega_m(s)\}_{m=1}^{m_{max}}$, where $m_{max} = F$ at stationary points and $F - 1$ at other points on the MEP; (iii) the determinant of the moment of inertia tensor, det $I(s)$.

A CVT/SCT calculation requires the above quantities plus the small-curvature effective reduced mass, $\mu^{SC}(s)$.

We have previously presented two basic formalisms for interpolating data for VTST/MT calculations: interpolated VTST[11,27] (IVTST) and VTST with interpolated corrections[14,19,28] (VTST-IC). In the IVTST approach the four items above are interpolated directly. In the VTST-IC approach we interpolate the deviation of a high-level result from a low-level result that is assumed to be available or calculable wherever we need it. The present article is devoted to the IVTST method, and we note that, in the new IVTST formalism presented here, which is called IVTST-M, an IVTST-M calculation may stand-alone as a self-contained single-level high-level calculation or may be used as the lower level of a VTST-IC dual-level calculation.

2.2. Algorithmic Preliminaries. In the present paper we assume that the reaction has a saddle point, and we choose this as the origin ($s = 0$) for s, with reactants at negative s and products at positive s. For interpolation on the reactant side of the saddle point of a bimolecular reaction, we have two choices. We may interpolate over the semi-infinite range between the reactant at $s = -\infty$ and the saddle-point region, or we may identify a local minimum (precursor complex) in this region and interpolate over the finite range between it and the saddle-point region. Similar considerations apply to the product side where we may or may not identify a successor complex. For interpolation on the reactant side of a unimolecular reaction or the product side of a reaction with one product, the interpolation is automatically over a finite range. The value of the reaction coordinate s is always measured in an isoinertial coordinate system[1−8] in which the kinetic energy is a diagonal quadratic form with reduced mass μ for every square term.

The procedures to be presented are systematically extendable to include more and more data. We use the notation IVTST-M-*H/G* to denote the number of energies, gradients, and Hessians employed. In IVTST-M-*H/G*, interpolations are based on optimized calculations of stationary points (reactants or precursor complex, saddle point, and product or successor complex) plus G additional energies and gradients, and H additional Hessians. The number G of gradient points is always equal to or larger than $H + 2$, since we will always assume that we will have at least one gradient point beyond the farthest Hessian point in each direction in order to estimate the curvature components at the farthest out Hessian points by double-side differentiation of the gradient. We assume that the G and H data are divided into G'' and H'' data on the reactant side and G' and H' data on the product side, where $G = G'' + G'$ and $H = H'' + H'$. Our procedure is defined when $G'' \geq 2$, $H'' \geq 1$, $G' \geq 2$, and $H' \geq 1$.

The leftmost and rightmost values of s on the grid of energies and gradients are denoted s_- and s_+, respectively.

A critical element in the schemes presented here is the use of splines under tension.[29,30] The use of spline interpolation methods allows us to obtain a continuous function, with continuous first and second derivatives, and the tension on the splines reduces the likelihood of spurious oscillations in the interpolated values. In addition, this approach is also applicable for any number of points for which the values of the function are known. All the interpolation by splines is carried out via the generally available splines-under-tension program package TSPACK.[30]

3. IVTST-M Interpolation Methods

This section gives procedures for single-level IVTST-M-*H*/*G*. In section 3.1 we will present the procedures used for mapping the reaction coordinate and interpolating the potential energy, $V_{MEP}(s)$. In section 3.2 are given the methods for interpolating the determinant of the moment of inertia tensor, det $I(s)$. Section 3.3 presents the interpolation of the vibrational frequencies. In section 3.4 we present the method used for the interpolation of the small-curvature effective reduced mass, $\mu^{SC}(s)$.

3.1. Mapping and Interpolation of the Potential Energy. According to the notation explained above, the energy along the reaction path will be available for G nonstationary points, plus the three stationary points, namely, reactants, products, and saddle point. The proposed interpolation scheme is based on a spline fit for which all input data are functions of the $G + 3$ energies that are available. The scheme will provide us with a function by which the energy is a continuous function of s, with continuous first and second derivatives. We will start by explaining our strategy for the case of a reaction that is bimolecular in both directions (two reactants and two products).

Before the spline fit is carried out, the independent variable of the function $V_{MEP}(s)$, that goes from $s = -\infty$ to $s = +\infty$, has to be mapped onto a finite interval, transforming an extrapolation problem into an interpolation problem. Thus, a change in variable is made, defining a new variable, z, as

$$z = \frac{2}{\pi}\arctan\left(\frac{s - s_0}{L}\right) \tag{1}$$

where the constants s_0 and L are estimated using the saddle-point properties. The new variable z allows us to map the function $V_{MEP}(s)$, defined in the interval $(-\infty,+\infty)$, onto a new function, $V_{MEP}(z)$, defined in the interval $[-1,+1]$.

The value of s_0 is calculated in such a way that the new function is centered in the area where the most important changes occur as the reaction takes place. If we define s_A^0 as the point on the reactant side of the reaction path with a value of $V_{MEP}(s)$ equal to half the barrier height measured from reactants and s_B^0 as the point on the product side with a potential energy equal to half the barrier height measured from products, the arithmetic average of s_A^0 and s_B^0 usually gives us the center of the interval of values of s where the most important changes in energy take place. However, this estimation procedure can lead to unphysical values of s_0 in the case of very exothermic or endothermic reactions. To avoid this kind of problem, we define new variables by

$$s_A = -\min(|s_A^0|, 2s_B^0) \tag{2}$$

$$s_B = \min(|s_A^0|, s_B^0) \tag{3}$$

The constant s_0 then given by

$$s_0 = (s_A + s_B)/2 \tag{4}$$

The constant L in eq 1 is a range parameter that is inversely related to the rate of change in the potential energy along the reaction path. Thus, it can be estimated by using the width of the reaction path as

$$L = (-|s_A| + s_B)/2 \tag{5}$$

Since it may be possible that the energy for the points along the reaction path is not available at s_A or s_B, to make the interpolation procedure consistent for any given value of G we will always estimate the distance to points halfway down the hill using a quadratic expansion based on the imaginary frequency at the saddle point. Thus

$$s_A^0 = -\sqrt{\frac{V_{MEP}(s=0) - V_{MEP}(s_R)}{|\omega^{\ddagger}|^2\mu}} \tag{6}$$

$$s_B^0 = -\sqrt{\frac{V_{MEP}(s=0) - V_{MEP}(s_P)}{|\omega^{\ddagger}|^2\mu}} \tag{7}$$

where μ is the reduced mass to which the coordinates of the system are scaled,[1-3] $\omega^{\ddagger}$ is the imaginary frequency at the saddle point, and s_R and s_P are the values of the reaction coordinate at reactants or products, i.e., $-\infty$ and $+\infty$ in the present case.

Once the mapping is finished, we have a set of $G + 3$ values of the energy as a function of z, in a range of values of z between $+1$ and -1. To obtain a physical interpolation even when the range spanned by the points for which the energy is available is not large, 10 extra energies are estimated between the reactants and the closest nonstationary point in the reactant channel, and similarly 10 extra energies are estimated between products and the last energy point in the product channel, to guide the spline interpolation in the tails of the reaction path. These 10 points are located at equally spaced points between $z = -1$ and the first point on the reaction path, and between the last point on the reaction path and $z = +1$.

The estimation of the energy for these 20 extra points is based on an Eckart potential. This function is defined by

$$V_{MEP}(s) = \frac{AY}{1+Y} + \frac{BY}{(1+Y)^2} + C \tag{8}$$

where

$$Y = \exp\left(\frac{s - s_0^{Eck}}{L^{Eck}(s)}\right) \tag{9}$$

$$A = V_{MEP}(s_P) - V_{MEP}(s_R) \tag{10}$$

$$C = V_{MEP}(s_R) \tag{11}$$

$$B = [2V_{MEP}(s=0) - A - 2C] \pm 2([V_{MEP}(s=0) - C][V_{MEP}(s=0) - A - C])^{1/2} \tag{12}$$

$$s_0^{Eck} = -L^{Eck}(s)\ln\left(\frac{(A+B)}{(B-A)}\right) \tag{13}$$

with $L^{Eck}(s)$ being a new function introduced for this step. The value of $L^{Eck}(s)$ is obtained for each nonstationary point by

fitting an Eckart potential that goes through the values of s and $V_{MEP}(s)$ for reactants, products, saddle point, and the nonstationary point in question, and with the maximum of $V_{MEP}(s)$ being constrained to be located at the saddle point. For the saddle point, this parameter is obtained from the imaginary frequency, according to

$$L^{Eck}(s{=}0) = \sqrt{\frac{2[V_{MEP}(s{=}0) - A]V_{MEP}(s{=}0)}{\mu|\omega^{\ddagger}|^2 B}} \quad (14)$$

Once we have $L^{Eck}(s)$ calculated for all the nonstationary points along the reaction path plus the saddle point, we map this function into the $[-1,+1]$ interval by again using eq 1, and we extrapolate the value of the two last $L^{Eck}(s)$ values on each side quadratically in order to obtain approximate values of $L^{Eck}(z)$ at $z = -1$ and $z = +1$. We then fit the function $L^{Eck}(z)$ by using splines under tension. Using this spline function, the value of s that corresponds to the variable z, and the energy of the stationary points, the Eckart potential will give us an approximate energy for each of these 20 extra points.

Once we have the set of $23 + G$ values of z and $V_{MEP}(z)$, a spline-under-tension fit to $V_{MEP}(z)$ is carried out, providing us with the energy along the reaction path for any desired value of s.

If the reaction has only one reactant and two products or two reactants and only one product, the same procedure can be applied for the bimolecular side of the reaction path. There are two differences when there is only one reactant and/or only one product. The first difference is that the interval of existence of z will be $[z(s_R),+1]$ if the reaction has one reactant at $s = s_R$ and two products, $[-1,z(s_P)]$ if the reaction has only one product located at $s = s_P$ and two reactants and $[z(s_R),z(s_P)]$ if there is one reactant and one product.

The second difference is the way we estimate the energy of the 10 extra points on the unimolecular side (or sides) of the reaction path. The procedure described above will only be valid for the bimolecular side, since it is based on an Eckart potential. For the unimolecular side a local cubic polynomial is substituted for the Eckart potential. In particular, we first consider 10 equally spaced values of s between s_R (or s_P) and the two closest nonstationary points, and we calculate their energy using a cubic polynomial fitted to the value of $V_{MEP}(s)$ at four points: the two closest nonstationary points, the value of s_R (or s_P), and an extra point at a distance δs from the reactant (or product), whose energy is approximated using the lowest frequency at the stationary point. (Note that δs is equal to the nominal step size of the reaction path algorithm that generates the G points where $V_{MEP}(s)$ is known on the path.) With these four pieces of information, we obtain the coefficients of a cubic polynomial that allows us to estimate the energy at 10 extra points. Then, we map the whole set of values of $V_{MEP}(s)$ and fit the function $V_{MEP}(z)$ for the $23 + G$ points using splines under tension.

Note that even if the reaction has only one reactant and one product, we still map $V_{MEP}(s)$ into an interval $[z(s_R),z(s_P)]$ and carry out the spline fit. Although the original set of data was already inside a finite interval, the mapping procedure is still carried out because the use of eqs 2−5 should lead to more physical interpolations.

If the reaction has two reactants or two products but there are wells in one or both of the reactant and product channels, the interpolating procedure can take advantage of the information about this stationary point. In that case, the interpolation may be done to the well, instead of the infinitely separated systems, following the same scheme for an unimolecular reaction. Wells, if present, can also be recognized for the case of one reactant or one product. If the location of wells is denoted as s_{RW} and s_{RP}, respectively, then the only change required in the above algorithm is the replacement of s_R by s_{RW} and/or s_P by s_{PW}. In general, except where stated otherwise it should be assumed that the interpolation is based on reactant or products data. However, we will test interpolation based on well properties in some cases because there exist systems where such a procedure would clearly be more physical. In general, the deeper the well with respect to reactants or products, the more likely is it that it is worthwhile to recognize it in the interpolation.

3.2. Interpolation of the Determinant of the Moment of Inertia. For interpolating the moment of inertia, the first step is to calculate the determinant of the moment of inertia at the G points for which the geometry is available. If the reaction has one reactant and/or one product, we also calculate the moment of inertia at these points; otherwise, we assume that its value is infinity at reactants or products. If one or two wells are recognized, their properties replace reactants and/or products. Once we have the values of $I(s)$ at $G + 3$ points, we map them into a finite interval using eq 1, obtaining the function $I(z)$. Since the moment of inertia changes with the square of the geometries and in order to eliminate its infinite value for bimolecular reactions and/or reactions with two products, we calculate the values of the function $1/\sqrt{I(Z)}$ for the $G + 3$ geometries. Since the values of this function are usually very small, its interpolation poses numerical problems. Thus, we scaled all the values of the function $1/\sqrt{I(Z)}$ by its value at the saddle point before spline-fitting it. The value of the moment of inertia for any point along the reaction path will be estimated by means of this spline fit.

3.3. Interpolation of the Frequencies along the Reaction Path. Frequencies for the $F - 1$ bound modes along the reaction path are interpolated by spline-fitting the function $\omega(z)$, calculated by using the H available values of $\omega(s)$ and eq 1. All the frequencies are interpolated by sorting them according to a canonical order; any allowed or avoided crossings and any symmetry constraints are, therefore, not taken into account. (Although this could be done in any individual case, it is not part of the present scheme, since it is hard to do automatically and consistently.) Imaginary frequencies are treated as negative numbers, and if the interpolation procedure results in negatives values for the frequencies, they are taken as imaginary.

The canonical order is as follows: Consider all $3N$ calculated frequencies. First put the six (five if linear) frequencies of smallest magnitude last. Then, for the remaining F frequencies, put the real ones first in order of decreasing magnitude followed by the imaginary ones in order of increasing magnitude. Ignore symmetry.

3.4. Interpolation of the Effective Reduced Mass for Small Curvature Tunneling. The effective reduced mass for small curvature tunneling, $\mu^{SC}(s)$, can be calculated using the expresion[5,6]

$$\mu^{SC} = \mu \prod_{m-1}^{F-1} f_m(s) \quad (15)$$

where

$$f_m(s) = \min\begin{Bmatrix}\exp\{-2\bar{a}(s) - [\bar{a}(s)]^2 + (d\bar{t}/ds)^2\} \\ 1\end{Bmatrix} \quad (16)$$

$$\bar{t} = (\kappa\hbar/\mu)^{1/2}\left(\sum_{m=1}^{F-1}[B_{mF}(s)]^2\omega_m{}^2(s)\right)^{-1/4} \quad (17)$$

$$\bar{a} = \kappa^{3/2}(\hbar/\mu)^{1/2}\left(\sum_{m=1}^{F-1}[B_{mF}(s)]^2\omega_m{}^2(s)\right)^{-1/4} \quad (18)$$

with κ being the magnitude of the curvature of the reaction path, and $B_{mF}(s)$ being one of the curvature components. The calculation of $B_{mF}(s)$ is carried out by methods explained previousy,[2,8,31] in particular as the scalar product of the s derivative of the gradient with the generalized normal-mode eigenvector. That eigenvector is calculated by the method of Miller *et al.*[32] when vibrations are treated in rectilinear coordinates and by the methods we presented elsewhere[8,31] when vibrations are treated in curvilinear coordinates. (Both coordinate systems are supported in our POLYRATE computer code,[33] but all calculations in the present paper employ curvilinear coordinates.)

The method adopted for interpolating μ^{SC} is to separately interpolate each curvature component along the reaction path. In particular, all the curvature components are interpolated using basically the same algorithm as for the frequencies and assuming they are zero at their asymptotic limits of reactants and products. However, there are two differences.

First, since curvature terms seem to vary over the range of the repulsive terms of the potential rather than the attractive ones, instead of using the constant L in eq 1, we use $L/2$, as recommended in ref 11.

Second, since curvature components usually decay rapidly as the system tends toward reactants or products, we raised the argument in eq 1 to a power. In particular, since curvature components usually peak quite sharply in certain areas of the reaction path, we modified the mapping procedure in order to make the curvature components change more rapidly than any other property. Thus, the mapping was carried out using the equation

$$z = \frac{2}{\pi}\arctan\left(\frac{s - s_0}{L/2}\right)^3 \quad (19)$$

An advantage of interpolating the curvature components is that when IVTST-M is used as the lower level of a dual-level calculation, one can combine the interpolated curvature components with corrected frequencies ω_m in eqs 17 and 18, thereby introducing further improvements in $\mu^{SC}(s)$. A second option is interpolating the argument of the exponential function in eq 16. Although we had some successes with this method, on the average it did not perform as well as interpolating the individual curvature components, and so we abandoned it.

4. Computational Details

The new IVTST-M interpolation algorithm was tested for a diverse set of test cases. Each test case is specified by a reaction and either an analytic potential energy function or a semiempirical or ab initio level of electronic structure theory. For every test case we first calculate converged rate constants by following the reaction path (using the Euler single-step method[1−3,26]) as far as necessary and by converging the calculations with respect to all step sizes. Then, we carried out IVTST-M calculations using much less data. To test the IVTST-M algorithm with standard parameters, we used a step size of $0.01a_0$ for all IVTST-M calculations except for the $Cl^- + CH_3Cl$ and $HBr + C_2H_2$ test cases, for which we used $0.003a_0$. According to the recommendations in previous work, the Hessian matrix was calculated every nine steps.[26] Since we always include one gradient point beyond the last Hessian on both sides of the saddle point in order to obtain $B_{mF}(s)$ by central differences, all tests will involve IVTST-M-*H*/*G* with $G \geq 9H + 2$. To minimize the number of cases considered, we limited attention to $G = 9n + 2$, where n is an integer greater than or equal to H. Rate constants were evaluated using CVT or ICVT, and tunneling was evaluated using both the ZCT and SCT methods.

The reduced mass μ to which all coordinates are scaled was always set either to 1 amu or to a value corresponding to one of the dominant physical motions in an important part of the reaction path. The later option was used for only one reaction, namely, $HBr + C_2H_2$, for which the scale mass was set to 26 amu.

For calculating the curvature along the reaction path at points where a Hessian is available, we used the gradient and the Hessian matrix at that point and the gradients at the closest points on both sides of it. The three gradients were fitted to a quadratic function, and the derivative of this function was calculated at the point where the Hessian is available for the calculation of the curvature components. If the Hessian point were the last point in the grid (so that gradients are available on only one side), the differentiation could be accomplished by one-sided difference; however, as explained above, we do not recommend this, and it will not be done in any of the calculations presented here. Several tests showed that the use of one-sided differences can lead to unphysical results when the last point on the grid has large-curvature components.

All the vibrational modes were treated harmonically, and the vibrational analysis was carried out using nonredundant[8,34,35] or redundant[31] internal coordinates. The internal coordinates that we included consisted of all the bond lengths and bond angles of the saddle point (including both the bond being formed and the bond being broken) plus a variable number of dihedral angles. For the $CH_3 + H_2$ reaction, no dihedral angles were required since the angle between the hydrogen approaching the CH_4, the hydrogen being abstracted, and the carbon atom has a value very close to 180° all along the reaction path, making a total number of five bond lengths and seven bond angles (one of them being a doubly degenerate linear bend). For the $OH + H_2$ reaction a dihedral angle, defined by the four atoms in the system, was also included, making a total of three bond lengths, two bond angles, and one dihedral angle. For the reaction $CH_4 + OH$, we assumed that the angle between the carbon, the hydrogen atom being abstracted, and the oxygen atom is almost linear, and we included three dihedral angles defined by the hydrogen atom in the OH, the oxygen and carbon atoms, and each of the three hydrogen atoms in the methyl group, making a total of six bond lengths, eight bond angles (one of them being a doubly degenerate linear bend), and three dihedral angles. In the calculations for the $Cl^- + CH_3Cl$ reaction, a dihedral angle defined by the carbon and the three hydrogen atoms was included in the calculation, making a total of 5 bond lengths, 10 bond angles (one of them being a doubly degenerate linear bend), and 1 dihedral angle. The pentadiene isomerization calculations involve 13 bond lengths, 21 bond angles (which are all the possible angles except the one formed by the hydrogen atom being transferred and the two carbons involved in the transfer, which was eliminated because of its unphysical meaning at large values of s), and 8 dihedral angles

TABLE 2: Estimated Value, s_R, of s, the Reaction Coordinate, at the Reactant Well ($OH\cdots H_2$) for the $OH + H_2 \rightarrow H_2O + H$ Reaction as a Function of the Location, s_-, of the Last Point on the Gradient Grid

s_- (a_0)	s_R (a_0)
accurate[a]	−2.41
−1.45	−2.35
−1.00	−2.25
−0.75	−2.21
−0.50	−2.18
−0.25	−2.15
−0.09	−2.14

[a] Calculated by following the reaction path all the way to the well.

which are all the possible dihedral angles that can be defined using two bonded carbon atoms and two hydrogen atoms, each one of them bonded to one of both carbon atoms. Finally, the coordinates employed in the study of the reaction $HBr + C_2H_2$ were the set of six bond lengths, six bond angles, and three dihedral angles described as set C in ref 31.

When the reaction has one or more stationary points (reactant, product, or well) with finite s values, Chen's method[36] was used for calculating its distance in isoinertial coordinates along a straight line from the farthest out gradient point on that side of the path. The value of s will therefore be dependent on the location of that reference point, and, consequently, it will depend on the extent of the calculated reaction path. Since this value affects the interpolation results, we checked the influence of the extent of the calculated reaction on the calculated s for the reactant well on the $OH + H_2 \rightarrow H_2O + H$ reaction with the Schatz−Elgersma[37] surface; see Table 2. As we reduce the extent of calculated reaction path, the estimated value of the distance to the well is not completely stable; rather it is reduced, as can be expected since we are measuring the distances along a straight line instead of along a curved reaction path. Nevertheless, this underestimation is not important, always being less than 12%.

The temperatures chosen for our study were 250, 300, and 2400 K for all the reactions except the $CH_3 + H_2$ reaction at the HF/STO-3G level, the 1,5-hydrogen shift in pentadiene, and the $HBr + C_2H_2$ reaction. These three reactions have very high barrier heights, so it was deemed more representative of realistic applications to study them at 400, 600, and 2400 K.

All the rate constants were originally calculated by using canonical variational theory (CVT). When tunneling is included, the classical adiabatic ground-state (CAG) factor,[1] with values ranging between 0 and 1, has to be included as a multiplicative factor. Nevertheless, as pointed out elsewhere,[1] a low value of the CAG factor might imply an inaccurate treatment of the thresholds. To avoid such problems, whenever the CAG factor was lower than 0.95 the improved CVT (ICVT) rate constant[1] was used. This only affects the cases 1 and 5, as well as the 4.1 and 4.4 cases when $H = 2$ and the case 7 when $G = 20$.

All the calculations were done using modified versions of the programs POLYRATE 7.4[33] and GAUSSRATE 7.4[38] programs. The latter is an interface of POLYRATE 7.4 and GAUSSIAN 94.[39] The new methods introduced in this paper will all be available in version 7.8.1 of POLYRATE.

A summary of the test cases is given in Table 3. The reactions used as test cases were $CH_3 + H_2 \rightarrow CH_4 + H$, $OH + H_2 \rightarrow H_2O + H$, $OH + CH_4 \rightarrow H_2O + CH_3$, $Cl^- + CH_3Cl \rightarrow CH_3Cl + Cl^-$, pentadiene isomerization, and $HBr + C_2H_2 \rightarrow H_2CCHBr$. The analytic potential energy surfaces employed were Joseph et al.'s J2 surface[40] for the $CH_3 + H_2 \rightarrow CH_4 + H$ reaction, the Schatz and Elgersma[37] surface for the $OH + H_2 \rightarrow H_2O + H$ reaction, based on the data by Walch and Dunning,[41] which will be denoted as WDSE, and the surface developed by Tucker and Truhlar[42] for the $Cl^- + CH_3Cl \rightarrow CH_3Cl + Cl^-$ reaction, which will be denoted as TT. The levels at which semiempirical calculations were performed are AM1[43] and PM3,[44] and the methods used for ab initio calculations were the Hartree−Fock method[45] (HF) and second-order Møller−Plesset perturbation theory[46] (MP2), with the minimum basis set STO-3G,[47] and the split-valence 3-21G basis set.[48] Note that since the purpose of this paper is methodology development, the accuracy of these potential surfaces (both the explicit analytic potential surfaces and implicit ones defined by a level of electronic structure theory) is not important. Rather these potential surfaces provide a way for us to compare IVTST-M calculations to calculations with converged values of H and G for the same potential energy surface and the same step-size δs.

5. Results

Tables 4−18 give the results. In each case we include a "cost" column. This is not an actual cost but rather the result of applying a generic cost function to get a rough idea of the relative costs of various calculations with components assigned costs that would be expected for a variety of typical applications. The generic cost C is given by

$$C = 2G + 7H + 12.5R + 25S \qquad (20)$$

where G denotes the number of nonstationary points at which an energy and a gradient is calculated, H denotes the number of these nonstationary points at which a Hessian is also calculated, 12.5 is an approximate cost for an optimization and final Hessian calculation on reactants or products, 25 is an approximate cost for a calculation in which the transition state or a well is optimized and its frequencies calculated, R denotes the number of calculations (two for an IVTST-M calculation and one for conventional transition-state theory) in which reactants or products are optimized and their final Hessians are calculated, and S denotes the number of calculations in which a transition state or well is optimized and its frequencies are calculated. Although eq 20 provides only a rough estimate of the expected relative cost in arbitrary units of various calculations, it does help to focus attention on the issue of cost, which is the motivation for this work.

5.1. $CH_3 + H_2 \rightarrow CH_4 + H$ Reaction, J2 Surface. The first reaction used for testing our new interpolation scheme was the reaction $CH_3 + H_2 \rightarrow CH_4 + H$, as described by the surface J2.[40] The results were converged with respect to G and H in an IVTST-M-36/326 calculation, and Table 4 shows the ratio to these converged rate constants as the number of points is reduced.

To better understand the performance of the method, we note some characteristics of this reaction. Variational effects are not very important for this reaction; thus, the ratio k^{TST}/k^{ICVT} is 1.65 at 250 K, with the transition state located at $s = -0.15a_0$, and as the temperature increases the transition state approaches the saddle-point ($s = 0$) location. Tunneling plays a moderate but quantitatively significant role, being a factor of 2.3 (ZCT) and 5.2 (SCT) at 250 K. The curvature of the reaction path shows typical behavior, with two minima and sharp changes at about $s = -0.2a_0$ and $+0.6a_0$.

Figure 1 shows the potential energy curve predicted by the IVTST-M-2/20, IVTST-M-6/56, and IVTST-M-10/92 schemes.

TABLE 3: Summary of Test Cases

case	reaction	potential surface	$V^{\ddagger a}$ (kcal)	ΔE^b (kcal)	no. of reactants	no. of products	well used R	well used P	$s_1{}^c$ (a_0)	$s_2{}^d$ (a_0)	well depth[a] R	well depth[a] P	s_- (a_0)	s_+ (a_0)	H'':H'
						Moderate-Barrier Reactions									
1	$CH_3 + H_2 \rightarrow CH_4 + H$	J2	9.9	−2.8	2	2	no	no	n/a[e]	n/a	n/a	n/a	−1.63	+1.63	1:1
2.1		MP2/3-21G	15.2	−8.3	2	2	no	no	n/a	n/a	n/a	n/a	−2.00	+1.00	1:1
2.2							no	no	n/a	n/a	n/a	n/a			2:1
2.3							no	yes	n/a	+6.4	n/a	−8.4			2:1
3.1	$OH + H_2 \rightarrow H_2O + H$	WDSE	6.1	−15.2	2	2	no	no	n/a	n/a	n/a	n/a	−1.00	+1.00	1:1
3.2							yes	no	−2.4	n/a	−1.3	n/a			1:1
4.1	$OH + CH_4 \rightarrow H_2O + CH_3$	AM1	10.6	−15.3	2	2	no	no	n/a	n/a	n/a	n/a	−1.36	+1.36	1:1
4.2							no	no	n/a	n/a	n/a	n/a			2:1
4.3							no	no	n/a	n/a	n/a	n/a			3:1
4.4							yes	no	−2.7	n/a	−1.3	n/a			1:1
4.5							yes	no	−2.7	n/a	−1.3	n/a			2:1
5	$Cl^- + CH_3Cl \rightarrow CH_3Cl + Cl^-$	TT	3.1	0.0	2	2	yes	yes	−5.2	+5.2	−11.0	−11.0	−0.975	+0.975	1:1
						High-Barrier Reactions									
6	$CH_3 + H_2 \rightarrow CH_4 + H$	HF/STO−3G	24.5	0.7	2	2	no	no	n/a	n/a	n/a	n/a	−1.54	+1.54	1:1
7	pentadiene isomerization	PM3	36.6	0.0	1	1	no	no	−30.3	+30.3	n/a	n/a	−1.27	+1.27	1:1
8	$HBr + C_2H_2 \rightarrow H_2CCHBr$	AM1	51.8	−26.4	2	1	no	no	n/a	+2.0	n/a	n/a	−0.3	+0.3	1:1

[a] Measured from reactants. [b] Classical endoergicity, that is, $V_{MEP}(s_P) - V_{MEP}(s_R)$. [c] Value of s at reactants (in unimolecular reactions) or reactant well (s_1 denotes s_R or s_{RW}). [d] Value of s at reactants (in unimolecular reactions) or reactant well (s_2 denotes s_P or s_{PW}). [e] n/a denotes not applicable.

TABLE 4: Ratio $k^{IVTST-M-H/G}/k^{IVTST-M-36/326}$ for the Reaction $CH_3 + H_2 \rightarrow CH_4 + H$, as Described by the J2 Surface

		ICVT			ICVT/ZCT			ICVT/SCT		
H/*G*	cost[a]	250 K	300 K	2400 K	250 K	300 K	2400 K	250 K	300 K	2400 K
2/20	104	1.14	1.10	1.00	1.91	1.60	1.01	3.86	3.01	1.03
2/38	140	1.14	1.10	1.00	1.33	1.26	1.01	1.39	1.40	1.02
2/56	176	1.14	1.10	1.00	1.33	1.27	1.01	1.43	1.42	1.02
2/74	212	1.14	1.10	1.00	1.32	1.26	1.01	1.42	1.41	1.01
2/92	248	1.14	1.10	1.00	1.32	1.26	1.01	1.42	1.41	1.01
2/146	356	1.14	1.10	1.00	1.32	1.26	1.01	1.42	1.41	1.01
2/200	464	1.14	1.10	1.00	1.32	1.26	1.01	1.42	1.41	1.01
2/308	682	1.14	1.10	1.00	1.32	1.26	1.01	1.42	1.41	1.01
4/38	154	1.00	1.00	1.00	1.42	1.30	1.01	1.43	1.39	1.01
4/56	190	1.00	1.00	1.00	1.42	1.30	1.01	1.44	1.39	1.01
4/74	226	1.00	1.00	1.00	1.41	1.29	1.01	1.42	1.38	1.01
4/92	262	1.00	1.00	1.00	1.41	1.29	1.01	1.41	1.38	1.01
4/146	370	1.00	1.00	1.00	1.41	1.29	1.01	1.41	1.36	1.01
4/200	478	1.00	1.00	1.00	1.41	1.29	1.01	1.41	1.36	1.01
4/308	694	1.00	1.00	1.00	1.41	1.29	1.01	1.41	1.36	1.01
6/56	204	1.00	1.00	1.00	1.31	1.21	1.00	1.44	1.34	1.01
6/74	240	1.00	1.00	1.00	1.31	1.20	1.00	1.42	1.33	1.01
6/92	276	1.00	1.00	1.00	1.31	1.20	1.00	1.41	1.33	1.01
6/308	708	1.00	1.00	1.00	1.30	1.20	1.00	1.41	1.32	1.01
8/74	254	1.00	1.00	1.00	1.20	1.12	1.00	1.39	1.28	1.00
8/92	290	1.00	1.00	1.00	1.19	1.12	1.00	1.38	1.27	1.00
8/308	722	1.00	1.00	1.00	1.19	1.12	1.00	1.38	1.27	1.00
10/92	304	1.00	1.00	1.00	1.12	1.07	1.00	1.32	1.21	1.00
10/146	412	1.00	1.00	1.00	1.12	1.07	1.00	1.32	1.21	1.00
10/200	520	1.00	1.00	1.00	1.12	1.07	1.00	1.32	1.21	1.00
10/308	736	1.00	1.00	1.00	1.12	1.07	1.00	1.32	1.21	1.00
16/146	454	1.00	1.00	1.00	1.02	1.01	1.00	1.10	1.05	1.00
16/200	562	1.00	1.00	1.00	1.02	1.01	1.00	1.11	1.05	1.00
16/308	778	1.00	1.00	1.00	1.02	1.01	1.00	1.11	1.05	1.00
22/200	604	1.00	1.00	1.00	1.00	1.00	1.00	1.02	1.01	1.00
22/308	820	1.00	1.00	1.00	1.00	1.00	1.00	1.02	1.01	1.00
34/308	922	1.00	1.00	1.00	1.00	1.00	1.00	1.00	1.00	1.00

[a] Assuming a cost of 1 for gradients and energy calculations, 7 for a Hessian calculation, and 50 for stationary-point optimizations and frequencies.

The figure shows that the reaction path energies predicted by IVTST-M-6/56 and IVTST-M-10/92 are in excellent agreement with the converged results, especially on the reactant side. On the product side the errors are larger, but are only significant at large distances from the saddle point where their influence is negligible even at 250 K. The IVTST-M-2/20 calculation

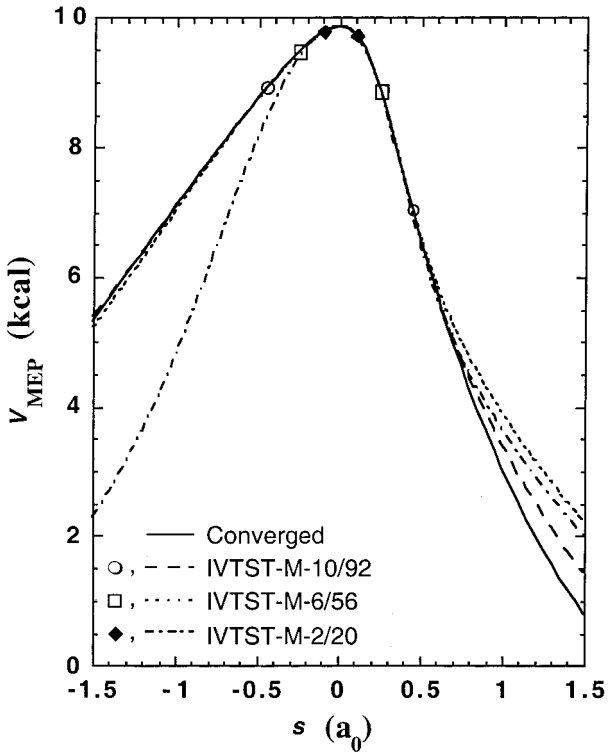

Figure 1. $V_{MEP}(s)$ for the $CH_3 + H_2 \rightarrow CH_4 + H$ reaction using the J2 surface as predicted by IVTST-M-2/20, IVTST-M-6/56, and IVTST-M-10/92. The converged results are shown for comparison. The symbols indicate the location of the last point included in each interpolation scheme.

significantly underestimates the energy on the reactant side and leads to significant deviations with respect to the converged results.

Figure 2 shows the $V_a{}^G$ curve, defined by

$$V_a{}^G(s) = V_{MEP}(s) + \frac{1}{2}\hbar\sum_{i=1}^{F-1}\omega_m(s) \qquad (21)$$

This curve plays a critical role in the tunneling calculations. Once again, IVTST-M-6/56 and IVTST-M-10/92 provide us with an excellent description on the reactant side of the reaction path, although more important deviations are observed in the

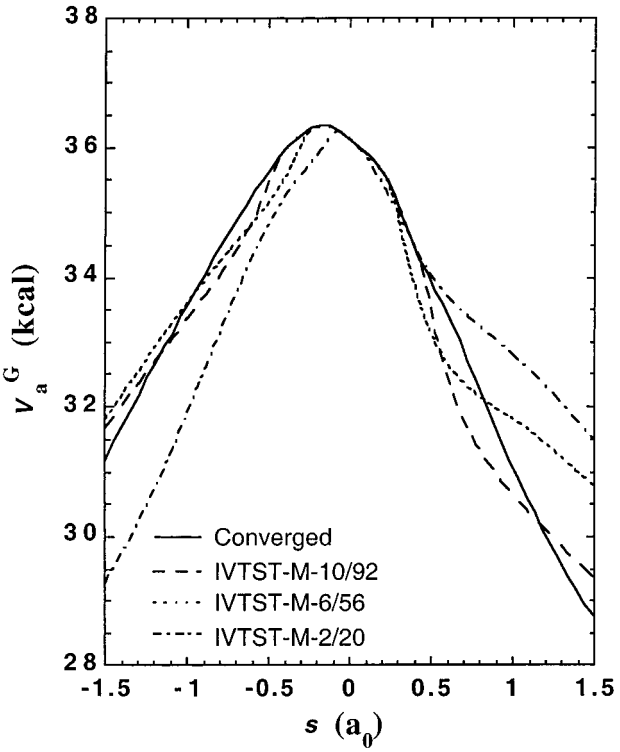

Figure 2. $V_a^G(s)$ for the $CH_3 + H_2 \rightarrow CH_4 + H$ reaction using the J2 surface as predicted by IVTST-M-2/20, IVTST-M-6/56, and IVTST-M-10/92. The converged results are shown for comparison.

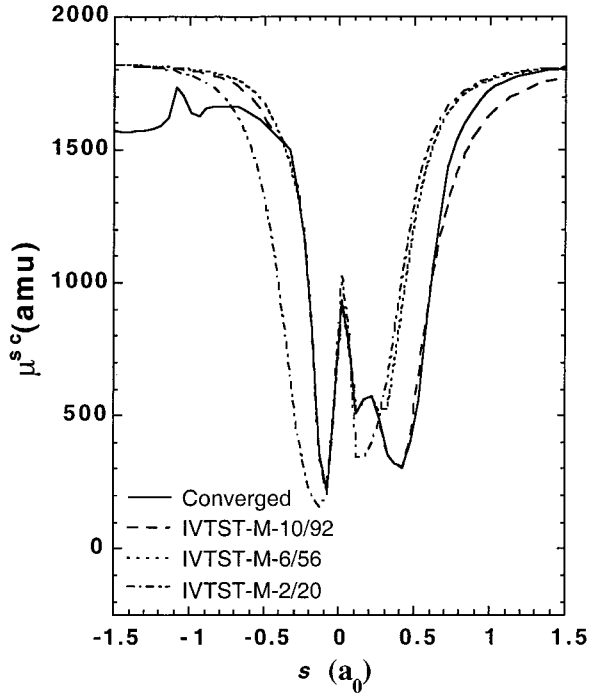

Figure 3. $\mu^{sc}(s)$ for the $CH_3 + H_2 \rightarrow CH_4 + H$ reaction using the J2 surface as predicted by IVTST-M-2/20, IVTST-M-6/56, and IVTST-M-10/92. The converged results are shown for comparison.

product side. The IVTST-M-6/56 scheme leads to a maximum error of roughly 2 kcal/mol at $s = +1.5a_0$, about $1.2a_0$ from the last point where uninterpolated information is available in that calculation. In general, the predicted V_a^G curve is in good agreement with the converged curve, leading to a good estimation of the ZCT tunneling. However, the IVTST-M-2/20 calculation underestimates the values of V_a^G on the reactant side as a consequence of the inaccuracies noted above in V_{MEP}. This scheme therefore leads to an effective barrier that is too narrow, and it overestimates the tunneling effects.

The analysis of the ICVT/ZCT columns in Table 4 implies that the agreement between the interpolated and actual frequencies and energies along the reaction path is good enough for quantitative dynamics calculations. Thus, the error in this calculation is always less than or equal to 42% when the number of points equals or exceeds the number used in the IVTST-M-2/38 calculation. It is interesting to note that the reduction in the number of Hessians available for the calculation increases the error even when the range of the reaction path for which Hessians are available is beyond the points where the curvature peaks, although the most important changes in the frequencies take place at these points. If the Hessians at these points are not included in the calculation, the frequencies have to be interpolated in the regions where they change suddenly, and the interpolation scheme is unable to predict such fast changes. As a consequence, when the information about frequencies is limited to about 10 points (between $s = -0.45a_0$ and $+0.45a_0$), the IVTST-M rate constants at 300 K have errors of at least 7%.

In Figure 3 the effective mass for SCT tunneling is plotted for the same H and G values as in the previous figures, and the ICVT/SCT columns of Table 4 reflect the effect of this interpolation on the rate constants. Although most of the error in the ICVT/SCT rate constant can be attributed to the miscalculation of the ZCT correction, those for the IVTST-M-2/20 case are due to the curvature. The overestimation of the curvature effects in the IVTST-M-2/20 calculation can be related to the deviations seen in the figure. Increasing H to 6 is already enough to correct most of the error. Thus, the error in the ICVT/SCT rate constant predicted with $H = 6$ is essentially the same as for the ICVT/ZCT calculation. The IVTST-M-10/92 calculation leads to a μ^{sc} plot that basically coincides with the converged result. The shallow peak in the reactant side at about $s = -1a_0$ is not predicted for any method since with the amount of information available the scheme cannot predict changes that take place so far from the last point included in the interpolation.

It is especially noteworthy that the use of a factor $L/2$ and an exponent set to 3 in the mapping procedure (eq 19) gives rise to curvature components that decay with about the right average rate.

Finally, in Table 4-S (in the Supporting Information) the rate constants are compared to a *fully* converged result, obtained with the ICVT/SCT method using a smaller gradient step size and Hessian step size. Those results show that only the ICVT/SCT rate constants can provide a reasonable description of the dynamics of the system, especially at low temperatures, where tunneling is very important and curvature effects must be included to obtain accurate results. In general, although we compared *all* calculations in this paper to results converged with respect to step sizes as well as the values of H and G (to be sure that our step sizes are reasonable choices), detailed comparisons of this type are not very informative with respect to judging the success of the mapping interpolation scheme. Thus, in the rest of section 5 we will continue to emphasize comparisons in which the potential surfaces and step size δs are both fixed; however, a full set of tests against fully converged results is given in the Supporting Information, and we will return to the question of full convergence in section 6.

This first test leads to ICVT/SCT results accurate to within 50% at 250 K using about 15% of the number of points required for a complete estimation of the rate constant without interpolation. Reduction of the number of Hessians leads to a loss of

TABLE 5: Ratio $k^{\text{IVTST-M-}H/G}/k^{\text{IVTST-M-33/299}}$ for the Reaction $CH_3 + H_2 \rightarrow CH_4 + H$, As Described by the MP2/3-21G Surface Using a 1:1 Distribution of Points on the Reactant and Product Sides

		CVT			CVT/ZCT			CVT/SCT		
		250	300	2400	250	300	2400	250	300	2400
H/*G*	cost[a]	K	K	K	K	K	K	K	K	K
2/20	104	1.00	1.00	1.00	0.95	1.29	1.01	0.40	0.73	1.02
2/38	140	1.00	1.00	1.00	1.51	1.63	1.02	0.75	1.06	1.02
2/56	176	1.00	1.00	1.00	1.64	1.70	1.02	0.84	1.13	1.02
2/74	212	1.00	1.00	1.00	1.58	1.67	1.02	0.79	1.10	1.02
2/92	248	1.00	1.00	1.00	1.52	1.65	1.02	0.75	1.08	1.02
2/146	356	1.00	1.00	1.00	1.50	1.65	1.02	0.73	1.07	1.02
2/200	464	1.00	1.00	1.00	1.50	1.65	1.02	0.73	1.07	1.02
4/38	154	1.01	1.00	1.00	2.32	2.00	1.01	1.50	1.71	1.02
4/56	190	1.00	1.00	1.00	2.56	2.10	1.01	1.70	1.85	1.02
4/74	226	1.00	1.00	1.00	2.47	2.08	1.01	1.61	1.81	1.02
4/92	262	1.01	1.00	1.00	2.38	2.06	1.01	1.53	1.77	1.02
4/146	370	1.01	1.00	1.00	2.36	2.04	1.01	1.50	1.75	1.02
4/200	478	1.01	1.00	1.00	2.36	2.05	1.01	1.51	1.75	1.02
6/56	204	1.00	1.00	1.00	2.38	1.78	1.00	2.07	1.92	1.01
6/74	240	1.00	1.00	1.00	2.29	1.75	1.00	1.97	1.87	1.01
6/92	276	1.00	1.00	1.00	2.23	1.74	1.00	1.87	1.83	1.01
6/146	384	1.00	1.00	1.00	2.20	1.72	1.00	1.82	1.81	1.01
6/200	492	1.00	1.00	1.00	2.21	1.73	1.00	1.83	1.81	1.01
8/74	254	1.00	1.00	1.00	1.86	1.44	1.00	1.83	1.62	1.00
8/92	290	1.00	1.00	1.00	1.81	1.42	1.00	1.75	1.58	1.00
8/146	398	1.00	1.00	1.00	1.78	1.42	1.00	1.70	1.56	1.00
8/200	506	1.00	1.00	1.00	1.79	1.42	1.00	1.71	1.57	1.00
10/92	304	1.00	1.00	1.00	1.49	1.24	1.00	1.58	1.40	1.00
10/146	412	1.00	1.00	1.00	1.47	1.24	1.00	1.53	1.38	1.00
10/200	520	1.00	1.00	1.00	1.48	1.24	1.00	1.56	1.39	1.00
12/146	426	1.00	1.00	1.00	1.29	1.14	1.00	1.38	1.25	1.00
12/200	534	1.00	1.00	1.00	1.30	1.14	1.00	1.40	1.26	1.00
14/146	440	1.00	1.00	1.00	1.18	1.08	1.00	1.26	1.16	1.00
14/200	548	1.00	1.00	1.00	1.19	1.08	1.00	1.28	1.17	1.00
16/146	454	1.00	1.00	1.00	1.11	1.04	1.00	1.18	1.10	1.00
16/200	562	1.00	1.00	1.00	1.12	1.04	1.00	1.20	1.11	1.00
18/200	576	1.00	1.00	1.00	1.07	1.02	1.00	1.14	1.07	1.00
20/200	590	1.00	1.00	1.00	1.04	1.01	1.00	1.10	1.04	1.00
22/200	604	1.00	1.00	1.00	1.02	1.00	1.00	1.06	1.02	1.00

[a] Assuming a cost of 1 for gradients and energy calculations, 7 for a Hessian calculation, and 50 for stationary-point optimizations and frequencies.

accuracy that cannot be compensated by an increase in the number of points for which the energy is calculated, making calculations with $G = 9H + 2$ more efficient than any calculations with extra gradient points. The reader should keep in mind that an error of 50% in the dynamical calculation is very reasonable, especially if compared to the errors introduced when we are forced to use lower levels of electronic structure calculations if we need a larger number of Hessians.

5.2. $CH_3 + H_2 \rightarrow CH_4 + H$ Reaction, MP2/3-21G Surface. Our second test is again based on the $CH_3 + H_2 \rightarrow CH_4 + H$ reaction; however, this time we base the potential energy surface on the MP2/3-21G level of theory. This reaction is exoergic by 8.3 kcal/mol, with a barrier of 15.2 kcal/mol.

The results for this test (Table 5) are consistent with our previous conclusions from the first test. Once again, it is more efficient to add extra Hessians rather than extra energy points to the data. Thus, the IVTST-M-10/92 calculation, with a computational cost of 304 units, gives better results than the IVTST-M-8/146, with a computational cost of 398 units, and only slightly worse results than IVTST-M-10/146, with the same number of Hessians and 54 more energies and a computational cost of 412 units.

Since this is an exothermic reaction, part of $V_{MEP}(s)$ in the product channel is located below the energy of reactants, having little or no influence in the calculation. Thus, the range in the product channel that needs to be taken into account can be smaller than the range in the reactant channel. In fact, a converged calculation shows us that the extent to which the reactant channel needs to be calculated is about 3 times larger than the product channel.

TABLE 6: Ratio $k^{\text{IVTST-M-}H/G}/k^{\text{IVTST-M-33/299}}$ for the Reaction $CH_3 + H_2 \rightarrow CH_4 + H$, As Described by the MP2/3-21G Surface Using a 2:1 Distribution of Points on the Reactant and Product Sides

		CVT			CVT/ZCT			CVT/SCT		
		250	300	2400	250	300	2400	250	300	2400
H/*G*	cost[a]	K	K	K	K	K	K	K	K	K
3/29	129	1.00	1.00	1.00	1.36	1.43	1.01	0.89	1.19	1.02
3/56	183	1.00	1.00	1.00	1.57	1.54	1.01	1.09	1.34	1.02
3/83	237	1.00	1.00	1.00	1.52	1.52	1.01	1.03	1.31	1.02
3/110	291	1.00	1.00	1.00	1.49	1.51	1.01	0.99	1.28	1.02
3/164	399	1.00	1.00	1.00	1.45	1.50	1.01	0.94	1.27	1.02
3/191	453	1.00	1.00	1.00	1.45	1.50	1.01	0.94	1.27	1.02
6/56	204	1.00	1.00	1.00	1.63	1.39	1.00	1.23	1.33	1.00
6/83	258	1.00	1.00	1.00	1.57	1.37	1.00	1.16	1.29	1.00
6/110	312	1.00	1.00	1.00	1.54	1.36	1.00	1.13	1.27	1.00
6/164	420	1.00	1.00	1.00	1.53	1.36	1.00	1.11	1.27	1.00
6/191	474	1.00	1.00	1.00	1.53	1.36	1.00	1.11	1.27	1.00
9/83	279	1.00	1.00	1.00	1.41	1.18	1.00	1.25	1.22	1.00
12/110	354	1.00	1.00	1.00	1.20	1.06	1.00	1.21	1.12	1.00
15/164	483	1.00	1.00	1.00	1.08	1.01	1.00	1.15	1.05	1.00
18/164	504	1.00	1.00	1.00	1.02	1.00	1.00	1.07	1.02	1.00
21/191	579	1.00	1.00	1.00	1.01	1.00	1.00	1.04	1.01	1.00

[a] Assuming a cost of 1 for gradients and energy calculations, 7 for a Hessian calculation, and 50 for stationary-point optimizations and frequencies.

We can take advantage of this fact in order to save some computer time. While for Table 5 the distribution of the effort in calculating reaction-path information in both channels was symmetric, in Table 6 we show calculations for this reaction in which we include twice the number of points on the reactant side as compared to the product side, thus extending the reaction path in the reactant channel twice as far as in the product channel. The asymmetric distribution of the number of points leads to good agreement with the converged rate constant at a slightly lower computational cost than when using a symmetric distribution. Thus, a symmetric IVTST-M-10/92 calculation, with a computational cost of 304, is less accurate than an asymmetric IVTST-M-9/83, with a computational cost of 279. For a computational cost of 204 units, a CVT/SCT rate constant at 250 K based on the IVTST-M-6/56 scheme is about a factor of 2 over the converged result when using a 1:1 distribution, while it is too high by just 23% when using a 2:1 distribution. It is reasonable to assume that one could take advantage of this asymmetry in routine applications since it is obvious from the exoergicity or from even a cursory examination of $V_{MEP}(s)$.

5.3. $CH_3 + H_2 \rightarrow CH_4 + H$ Reaction, MP2/3-21G Surface, Using the Product Side Well. The MP2/3-21G surface has a very loose minimum on the product side of the reaction, only about 0.06 kcal/mol below the products energy. By interpolating the product side using the unimolecular scheme described in section 3, we have tested the effect of including structural, energetic, and frequency information for this minimum in our calculation of the rate constant for the $CH_3 + H_2$ reaction. The distribution of points was taken in an asymmetric fashion as discussed above. The results are shown in Table 7.

When including more than 56 energy and gradient points, the interpolation including well information slightly improves the results. Nevertheless, when the amount of information is reduced, the interpolation based on product properties yields better results. Anyway, the differences are not very large,

TABLE 7: Ratio $k^{\text{IVTST-M-}H/G}/k^{\text{IVTST-M-33/299}}$ for the Reaction $CH_3 + H_2 \rightarrow CH_4 + H$, As Described by the MP2/3-21G Surface Using $H'':H'$ :: 2:1 and Interpolating on the Product Side by Using the $CH_4\cdots H$ Well

		CVT			CVT/ZCT			CVT/SCT		
H/*G*	cost[a]	250 K	300 K	2400 K	250 K	300 K	2400 K	250 K	300 K	2400 K
3/29	154	1.00	1.00	1.00	0.08	0.30	1.00	0.02	0.09	0.99
3/56	208	1.00	1.00	1.00	0.62	1.00	1.01	0.29	0.63	1.02
3/83	262	1.00	1.00	1.00	1.24	1.39	1.01	0.77	1.12	1.02
3/110	316	1.00	1.00	1.00	1.42	1.47	1.01	0.95	1.24	1.02
3/164	424	1.00	1.00	1.00	1.40	1.46	1.01	0.91	1.23	1.02
3/191	478	1.00	1.00	1.00	1.39	1.46	1.01	0.90	1.22	1.02
6/56	229	1.00	1.00	1.00	0.77	1.01	1.00	0.42	0.74	1.00
6/83	283	1.00	1.00	1.00	1.35	1.29	1.00	0.93	1.15	1.00
6/110	337	1.00	1.00	1.00	1.49	1.34	1.00	1.08	1.24	1.00
6/164	445	1.00	1.00	1.00	1.48	1.34	1.00	1.07	1.24	1.00
6/191	499	1.00	1.00	1.00	1.48	1.34	1.00	1.06	1.24	1.00
9/83	304	1.00	1.00	1.00	1.27	1.14	1.00	1.06	1.13	1.00
12/110	379	1.00	1.00	1.00	1.20	1.05	1.00	1.20	1.12	1.00
15/164	508	1.00	1.00	1.00	1.08	1.01	1.00	1.15	1.05	1.00
18/164	529	1.00	1.00	1.00	1.02	1.00	1.00	1.07	1.02	1.00
21/191	604	1.00	1.00	1.00	1.01	1.00	1.00	1.05	1.01	1.00

[a] Assuming a cost of 1 for gradients and energy calculations, 7 for a Hessian calculation, and 75 for stationary-point optimizations and frequencies.

TABLE 8: Ratio $k^{\text{IVTST-M-}H/G}/k^{\text{IVTST-M-32/290}}$ for the Reaction $OH + H_2 \rightarrow H_2O + H$, As Described by the WDSE Surface

		CVT			CVT/ZCT			CVT/SCT		
H/*G*	cost[a]	250 K	300 K	2400 K	250 K	300 K	2400 K	250 K	300 K	2400 K
2/20	104	1.39	1.31	1.03	1.74	1.69	1.04	1.56	1.62	1.04
2/38	140	1.38	1.30	1.03	1.99	1.83	1.04	1.91	1.86	1.04
4/38	144	0.99	0.99	1.00	1.61	1.50	1.01	1.53	1.53	1.01
4/56	190	0.99	0.99	1.00	1.73	1.57	1.01	1.71	1.64	1.01
6/56	204	1.00	1.00	1.00	1.38	1.30	1.01	1.38	1.36	1.01
6/74	240	1.00	1.00	1.00	1.34	1.27	1.01	1.32	1.32	1.01
8/74	244	1.00	1.00	1.00	1.15	1.13	1.00	1.12	1.14	1.00
8/92	290	1.00	1.00	1.00	1.19	1.15	1.00	1.19	1.19	1.00
10/92	304	1.00	1.00	1.00	1.08	1.06	1.00	1.06	1.08	1.00
14/146	440	1.00	1.00	1.00	1.03	1.02	1.00	1.03	1.03	1.00
16/146	454	1.00	1.00	1.00	1.00	1.00	1.00	1.00	1.00	1.00
20/200	590	1.00	1.00	1.00	1.00	1.00	1.00	1.00	1.00	1.00
22/200	604	1.00	1.00	1.00	1.00	1.00	1.00	1.00	1.00	1.00

[a] Assuming a cost of 1 for gradients and energy calculations, 7 for a Hessian calculation, and 50 for stationary-point optimizations and frequencies.

probably due to the large separation between the saddle point and the well ($6.4a_0$) and its small stabilization energy (0.06 kcal/mol), as well as the relatively small importance of the product side in this exothermic reaction. As a consequence, the interpolation to the separate products or to the well makes little difference. It is a mark in favor of our new method that it shows this insensitivity.

5.4. $OH + H_2 \rightarrow H_2O + H$ Reaction, WDSE Surface. The next reaction under study is the abstraction of a hydrogen atom from the hydrogen molecule by the hydroxyl radical, described by using the WDSE potential energy surface.

This reaction has significant variational effects, with the ratio $k^{\text{TST}}/k^{\text{CVT}}$ equaling 3.75 at 250 K. Tunneling is also important, being a factor of 28.8 at 250 K according to the SCT calculation.

In Table 8 are shown the ratios between the interpolated rate constants and the limits to which the interpolated rate constants tend as *H* and *G* are increased. The conclusions are very similar to those in the previous examples. Increasing the number of points for which the energy is known without increasing the number of Hessians does not improve the results. The methods with $H = 9G + 2$ are therefore more efficient than the others.

It is noteworthy that the interpolation procedure recovers most of the variational effects even with very little information about the Hessians along the reaction path.

TABLE 9: Ratio $k^{\text{IVTST-M-}H/G}/k^{\text{IVTST-M-32/290}}$ for the Reaction $OH + H_2 \rightarrow H_2O + H$, As Described by the WDSE Surface, Using the $OH\cdots H_2$ Well for Interpolation on the Reactant Side

		CVT			CVT/ZCT			CVT/SCT		
H/*G*	cost[a]	250 K	300 K	2400 K	250 K	300 K	2400 K	250 K	300 K	2400 K
2/20	129	1.38	1.29	1.03	0.61	0.78	1.03	0.35	0.53	1.03
2/38	165	1.38	1.29	1.03	0.92	1.06	1.05	0.60	0.80	1.04
4/38	179	1.00	1.00	1.00	0.81	0.94	1.00	0.57	0.74	1.00
4/56	215	1.00	1.00	1.00	1.01	1.10	1.00	0.77	0.93	1.00
6/56	229	1.00	1.00	1.00	0.90	0.99	1.00	0.72	0.86	1.00
6/74	265	1.00	1.00	1.00	1.02	1.07	1.00	0.86	0.98	1.00
8/74	279	1.00	1.00	1.00	0.95	1.01	1.00	0.82	0.93	1.00
8/92	315	1.00	1.00	1.00	1.01	1.05	1.00	0.92	1.00	1.00
10/92	329	1.00	1.00	1.00	0.98	1.01	1.00	0.89	0.97	1.00
14/146	465	1.00	1.00	1.00	1.01	1.01	1.00	1.00	1.01	1.00
16/146	479	1.00	1.00	1.00	1.00	1.00	1.00	0.99	1.00	1.00
20/200	615	1.00	1.00	1.00	1.00	1.00	1.00	1.01	1.00	1.00
22/200	629	1.00	1.00	1.00	0.99	1.00	1.00	0.98	0.99	1.00

[a] Assuming a cost of 1 for gradients and energy calculations, 7 for a Hessian calculation, and 75 for stationary-point optimizations and frequencies.

It is noteworthy that the interpolation procedure recovers most of the variational effects even with very little information about the Hessians along the reaction path.

5.5. $OH + H_2 \rightarrow H_2O + H$ Reaction, WDSE Surface, Using the Reactant Well. The WDSE analytical potential energy surface has a 1.3 kcal/mol deep well in the reactant channel, located at about $s = -2.4a_0$.

Table 9 show the results of IVTST-M calculations in which the interpolation uses information about this well. Use of this information leads to rate constants that converge faster to the limit of the largest calculation. It is reasonable that the unimolecular interpolation scheme is more efficient since no extrapolation to an infinitely separated reactant has to be done (in fact, this was our motivation for recognizing wells). In this case it has to be noted that an increase in the number of energy data without increasing the amount of Hessian data does lead to results closer to the converged ones, especially when using a small number of points. Thus, the error in the rate constant at 250 K is reduced significantly when improving the calculation from IVTST-M-2/20 to IVTST-M-2/38.

5.6. $OH + CH_4 \rightarrow CH_3 + H_2O$ Reaction, AM1 Surface. Variational effects are very important for the $OH + CH_4$ reaction on the AM1 surface, and they diminish the rate constant by a factor of 9 with respect to the TST value at 250 K, with the factor decreasing to 7 at 300 K and 5 at 2400 K. The transition state is located at about $s = -0.26a_0$ for all the temperatures, and it is out of the range of values for which Hessian information is available when $H'' < 3$. The results for this reaction are shown in Table 10. The interpolation procedure predicts a variational effect of 2.5 at 250 K when $H'' = 1$, increasing to 5 when $H'' = 2$, and reaching the correct value for bigger values of H''.

The error in the CVT/ZCT rate constant is in great part due to the error in the CVT rate constant, agreeing very well with the converged results for $H \geq 6$. The effect of reaction-path curvature requires a larger amount of data to converge well.

Since the reaction is quite exothermic (by 15.2 kcal), it can be expected that a more efficient calculation would be to take 2 or 3 times as many points on the reactant side as in the product

TABLE 10: Ratio $k^{IVTST-M-H/G}/k^{IVTST-M-30/272}$ for the Reaction OH + CH_4 → H_2O + CH_3, As Described by the AM1 Surface, Using H'':H' :: 1:1[a]

		VTST			VTST/ZCT			VTST/SCT		
H/*G*	cost[b]	250 K	300 K	2400 K	250 K	300 K	2400 K	250 K	300 K	2400 K
2/20	104	3.96	3.22	2.05	5.78	4.96	2.00	1.30	1.65	1.96
2/38	140	3.97	3.22	1.86	2.62	2.98	1.90	0.48	0.84	1.86
4/38	154	2.07	1.83	1.32	1.88	2.09	1.33	0.77	1.13	1.32
4/56	190	2.07	1.83	1.32	3.13	2.84	1.33	1.65	1.91	1.33
6/56	204	1.01	1.01	1.01	1.44	1.44	1.01	1.38	1.58	1.03
6/74	240	1.01	1.01	1.01	1.98	1.71	1.01	2.27	2.23	1.03
8/74	254	1.01	1.01	1.00	1.45	1.32	1.01	1.45	1.49	1.01
8/92	290	1.01	1.01	1.00	1.54	1.36	1.01	1.59	1.58	1.01
10/92	304	1.00	1.00	1.00	1.13	1.10	1.00	1.02	1.10	1.00
10/110	340	1.00	1.00	1.00	1.23	1.14	1.00	1.19	1.21	1.00
12/110	354	1.00	1.00	1.00	1.12	1.08	1.00	1.07	1.10	1.00
14/146	440	1.00	1.00	1.00	1.15	1.07	1.00	1.20	1.16	1.00
16/146	454	1.00	1.00	1.00	0.98	1.00	1.00	0.91	0.98	1.00
20/200	590	1.00	1.00	1.00	1.00	1.00	1.00	0.98	1.00	1.00
22/200	604	1.00	1.00	1.00	0.98	0.99	1.00	0.93	0.97	1.00

[a] VTST denotes ICVT for $H = 2$ and CVT for $H \geq 4$ (see section 4). [b] Assuming a cost of 1 for gradients and energy calculations, 7 for a Hessian calculation, and 50 for stationary-point optimizations and frequencies.

TABLE 11: Ratio $k^{IVTST-M-H/G}/k^{IVTST-M-33/299}$ for the Reaction OH + CH_4 → H_2O + CH_3, As Described by the AM1 Surface, Using H'':H' :: 2:1

		CVT			CVT/ZCT			CVT/SCT		
H/*G*	cost[a]	250 K	300 K	2400 K	250 K	300 K	2400 K	250 K	300 K	2400 K
3/29	129	2.08	1.84	1.33	1.77	2.03	1.32	0.72	1.08	1.31
3/56	183	2.08	1.84	1.33	3.84	3.17	1.33	2.43	2.44	1.33
6/56	204	1.01	1.01	1.00	1.45	1.32	1.01	1.44	1.48	1.01
6/83	258	1.01	1.01	1.00	1.67	1.42	1.01	1.85	1.73	1.01
9/83	279	1.00	1.00	1.00	1.13	1.08	1.00	1.06	1.10	1.00
9/110	333	1.00	1.00	1.00	1.17	1.09	1.00	1.17	1.16	1.00
12/110	354	1.00	1.00	1.00	0.98	1.00	1.00	0.91	0.98	1.00
15/164	483	1.00	1.00	1.00	1.01	1.00	1.00	1.00	1.01	1.00
18/164	504	1.00	1.00	1.00	1.00	1.00	1.00	0.98	0.99	1.00

[a] Assuming a cost of 1 for gradients and energy calculations, 7 for a Hessian calculation, and 50 for stationary-point optimizations and frequencies.

TABLE 12: Ratio $k^{IVTST-M-H/G}/k^{IVTST-M-33/299}$ for the Reaction OH + CH_4 → H_2O + CH_3, As Described by the AM1 Surface, Using H'':H :: 3:1

		CVT			CVT/ZCT			CVT/SCT		
H/*G*	cost[a]	250 K	300 K	2400 K	250 K	300 K	2400 K	250 K	300 K	2400 K
4/38	154	1.01	1.01	1.01	1.34	1.38	1.01	1.28	1.49	1.03
4/74	226	1.01	1.01	1.01	2.08	1.74	1.01	2.74	2.48	1.03
8/74	254	1.00	1.00	1.00	1.12	1.07	1.00	1.06	1.10	1.00
8/110	326	1.00	1.00	1.00	1.20	1.10	1.00	1.24	1.19	1.00
12/110	354	1.00	1.00	1.00	0.97	0.99	1.00	0.91	0.96	1.00
12/146	426	1.00	1.00	1.00	1.00	1.00	1.00	0.98	1.00	1.00
16/146	454	1.00	1.00	1.00	1.00	1.00	1.00	0.99	0.99	1.00
16/182	526	1.00	1.00	1.00	1.02	1.00	1.00	1.04	1.01	1.00
20/182	554	1.00	1.00	1.00	1.01	1.00	1.00	1.02	1.01	1.00

[a] Assuming a cost of 1 for gradients and energy calculations, 7 for a Hessian calculation, and 50 for stationary-point optimizations and frequencies.

side. These results are shown in Tables 11 and 12. However, the improvement is not very great. Thus, rate constants of the quality of a IVTST-M-10/92 calculation with a ratio of 1:1 between points on the reactant and product sides are obtained with an IVTST-M-9/83 calculation using the 2:1 proportion, reducing the computational cost by only about 8%. The results

TABLE 13: Ratio $k^{IVTST-M-H/G}/k^{IVTST-M-30/272}$ for the Reaction OH + CH_4 → H_2O + CH_3, As Described by the AM1 Surface, Using H'':H' :: 1:1 and Basing the Interpolation on the Reactant Side on the CH_4···OH Well[a]

		VTST			VTST/ZCT			VTST/SCT		
H/*G*	cost[b]	250 K	300 K	2400 K	250 K	300 K	2400 K	250 K	300 K	2400 K
2/20	129	4.05	3.27	1.49	2.42	2.59	1.49	0.53	0.82	1.45
2/38	165	4.05	3.27	1.50	4.26	3.87	1.50	1.02	1.34	1.48
4/38	179	2.36	2.04	1.33	3.69	3.11	1.31	2.07	2.21	1.31
4/56	215	2.36	2.04	1.33	3.04	2.74	1.31	1.62	1.84	1.31
6/56	229	1.03	1.03	1.01	1.81	1.62	1.02	1.95	1.99	1.03
6/74	265	1.03	1.03	1.01	1.89	1.67	1.02	2.07	2.09	1.04
8/74	279	1.00	1.00	1.00	1.52	1.34	1.00	1.56	1.55	1.02
8/92	315	1.00	1.00	1.00	1.64	1.40	1.00	1.73	1.68	1.01
10/92	329	1.00	1.00	1.00	1.29	1.17	1.00	1.28	1.26	1.00
10/110	369	1.00	1.00	1.00	1.36	1.20	1.00	1.38	1.34	1.00
12/110	379	1.00	1.00	1.00	1.25	1.12	1.00	1.28	1.23	1.00
14/146	465	1.00	1.00	1.00	1.28	1.12	1.00	1.44	1.29	1.00
16/146	479	1.00	1.00	1.00	1.10	1.04	1.00	1.18	1.12	1.00
20/200	615	1.00	1.00	1.00	1.06	1.02	1.00	1.13	1.07	1.00
22/200	629	1.00	1.00	1.00	1.02	1.01	1.00	1.06	1.03	1.00

[a] VTST denoted ICVT for $H = 2$ and CVT for $H \geq 4$ (see section 4). [b] Assuming a cost of 1 for gradients and energy calculations, 7 for a Hessian calculation, and 50 for stationary-point optimizations and frequencies.

TABLE 14: Ratio $k^{IVTST-M-H/G}/k^{IVTST-M-9/299}$ for the Reaction OH + CH_4 → H_2O + CH_3, As Described by the AM1 Surface, Using H'':H' :: 2:1 and Basing the Interpolation on the Reactant Side on the CH_4···OH Well

		CVT			CVT/ZCT			CVT/SCT		
H/*G*	cost[a]	250 K	300 K	2400 K	250 K	300 K	2400 K	250 K	300 K	2400 K
3/29	154	2.40	2.07	1.33	3.22	2.86	1.32	1.87	2.02	1.32
3/56	208	2.39	2.07	1.33	2.89	2.65	1.31	1.63	1.82	1.31
6/56	229	1.00	1.00	1.00	1.51	1.34	1.00	1.55	1.54	1.01
6/83	283	1.00	1.00	1.00	1.71	1.44	1.00	1.86	1.74	1.01
9/83	304	1.00	1.00	1.00	1.25	1.12	1.00	1.29	1.23	1.00
9/110	358	1.00	1.00	1.00	1.33	1.15	1.00	1.43	1.31	1.00
12/110	379	1.00	1.00	1.00	1.10	1.04	1.00	1.17	1.10	1.00
15/164	508	1.00	1.00	1.00	1.06	1.02	1.00	1.14	1.06	1.00
18/164	529	1.00	1.00	1.00	1.03	1.01	1.00	1.07	1.02	1.00

[a] Assuming a cost of 1 for gradients and energy calculations, 7 for a Hessian calculation, and 75 for stationary-point optimizations and frequencies.

of a 3:1 distribution show similar trends, although the savings in computational costs are greater than when using a 2:1 proportion.

5.7. OH + CH_4 → CH_3 + H_2O Reaction, AM1 Surface, Using the Reactant Side Well. The AM1 surface for the reaction between methane and OH has a well on the reactant side. Table 13 shows that including this well does not make the convergence faster, and the same cost is required.

The calculations were repeated using an asymmetrical distribution of the information along the reaction path. The results are shown in Table 14. Once again, the asymmetrical distribution only slightly reduces the computational cost of a converged calculation. Although an asymmetric distribution of data does not always result in significant improvement, it does not seem to make the results worse either, and so it is probably to be recommended as the most efficient procedure for significantly exoergic reactions.

5.8. Cl^- + CH_3Cl → $ClCH_3$ + Cl^- Reaction, TT Surface. The analytical surface developed by Tucker and Truhlar for the Cl^- + CH_3Cl S_N2 reaction has deep wells in both the reactant and product channels, and so these were used for the interpola-

TABLE 15: Ratio $k^{\text{IVTST-M-}H/G}/k^{\text{IVTST-M-14/128}}$ for the Reaction $Cl^- + CH_3Cl \rightarrow CH_3Cl + Cl^-$, As Described by the TT Surface, Basing the Interpolation on Both Reactant and Product Sides on the Ion−Dipole Wells

		ICVT			ICVT/ZCT			ICVT/SCT		
H/G	cost[a]	250 K	300 K	2400 K	250 K	300 K	2400 K	250 K	300 K	2400 K
2/20	154	1.01	1.01	0.73	0.82	0.88	0.73	1.83	1.55	0.74
2/38	190	1.01	1.01	0.74	0.84	0.89	0.74	1.99	1.64	0.75
4/38	204	1.00	1.00	0.82	0.86	0.90	0.82	0.98	0.98	0.82
4/56	240	1.00	1.00	0.83	0.88	0.92	0.83	1.02	1.01	0.83
6/56	254	1.00	1.00	0.88	0.90	0.93	0.87	0.93	0.95	0.87
6/74	290	1.00	1.00	0.89	0.92	0.94	0.89	0.96	0.97	0.89
8/74	304	1.00	1.00	0.92	0.93	0.96	0.92	0.93	0.96	0.92
8/92	340	1.00	1.00	0.93	0.95	0.96	0.93	0.95	0.97	0.93
10/92	354	1.00	1.00	0.95	0.96	0.97	0.95	0.95	0.97	0.95
10/110	390	1.00	1.00	0.97	0.98	0.99	0.96	0.98	0.98	0.96
12/110	404	1.00	1.00	0.99	0.98	0.99	0.99	0.98	0.98	0.99
12/128	440	1.00	1.00	1.00	0.99	1.00	1.00	0.99	1.00	1.00
14/128	454	1.00	1.00	1.00	1.00	1.00	1.00	1.00	1.00	1.00

[a] Assuming a cost of 1 for gradients and energy calculations, 7 for a Hessian calculation, and 100 for stationary-point optimizations and frequencies.

tion. (We recommend that one always recognize deep wells, whereas recognition of shallow van der Waals wells is optional.) The barrier height is 3.1 kcal/mol, with variational effects being almost negligible (less than 5% of difference between TST and CVT for the temperature range under study) and tunneling not having a very large contribution (a factor of 1.8 at 200 K calculated using SCT).

The main problem with this reaction is the difficulty in obtaining a converged reaction path. When using a reduced mass of 1 amu, the step-size used in all the previous tests, $0.01a_0$, was too big for obtaining an accurate reaction path. The step size was therefore reduced to $0.003a_0$, keeping the factor of 9 for each Hessian calculation. Thus, since the most important problem we have to solve in our interpolation schemes is to reach the areas where significant changes take place, the reduction of the step size could conceivably require an increase in the number of points (and computational cost) in the calculation in order to get an accurate result.

Table 15 shows the results. The low tunneling effects and lack of variational effects makes the agreement very good even for H as small as 4, although the errors in the interpolation of V_{MEP} and frequencies are additive, leading to an overestimation of variational effects at high temperatures, which causes an underestimation of the ICVT, ICVT/ZCT and ICVT/SCT, rate constants at 2400 K by more than 15%.

5.9. $CH_3 + H_2 \rightarrow CH_4 + H$ Reaction, HF/STO-3G Surface. An HF/STO-3G calculation for $CH_3 + H_2$ reaction leads to an almost symmetric and very high barrier (endoergicity is 0.7 kcal/mol and the barrier height is 24.5 kcal/mol). The variational transition state can be considered to be located at the saddle point over the range of temperatures we studied, but as a consequence of the high, narrow barrier, tunneling contributions are very important, being a factor of about 200 at 400 K, according to the SCT values. A small deviation of the interpolated energies or frequencies from the converged values leads to a very different estimation of the tunneling correction.

The results for this tests appear in Table 16. The trends are similar to those observed in previous tests.

5.10. 1,5-Hydrogen Shift in 1,3-Pentadiene, PM3 Surface. This is another extremely hard test of our interpolation scheme because of the unusual shape of the barrier. If we start going downhill to reactants and products from the saddle point, we find that at $s = \pm 3.0a_0$, the energy along the reaction path has fallen about 30 kcal/mol, to around 6 kcal/mol. Reactants are estimated to be at a distance of about $30a_0$ from the saddle point, since the full reaction path involves low-energy wide-amplitude motion of a methyl group. Consequently, the barrier, although extremely thin near the saddle point, is very broad as we get farther from the saddle point. Using information about only areas near the saddle point has the consequence of predicting a too broad barrier which severely underestimates the tunneling factor.

TABLE 16: Ratio $k^{\text{IVTST-M-}H/G}/k^{\text{IVTST-M-34/308}}$ for the Reaction $CH_3 + H_2 \rightarrow CH_4 + H$, As Described by the HF/STO-3G Surface

		CVT			CVT/ZCT			CVT/SCT		
H/G	cost[a]	400 K	600 K	2400 K	400 K	600 K	2400 K	400 K	600 K	2400 K
2/20	104	1.00	1.00	1.00	2.19	1.36	1.01	0.61	0.88	1.00
2/38	140	1.00	1.00	1.00	1.66	1.28	1.01	0.41	0.79	0.99
4/38	154	1.00	1.00	1.00	2.32	1.34	1.01	1.22	1.24	1.01
4/56	190	1.00	1.00	1.00	2.22	1.33	1.01	1.12	1.22	1.01
6/56	204	1.00	1.00	1.00	1.75	1.13	1.00	2.18	1.43	1.01
6/74	240	1.00	1.00	1.00	1.74	1.13	1.00	2.05	1.43	1.01
8/74	254	1.00	1.00	1.00	1.28	1.03	1.00	1.82	1.20	1.00
8/92	290	1.00	1.00	1.00	1.27	1.03	1.00	1.71	1.19	1.00
10/92	304	1.00	1.00	1.00	1.08	1.01	1.00	1.48	1.08	1.00
10/110	340	1.00	1.00	1.00	1.08	1.01	1.00	1.49	1.08	1.00
12/110	354	1.00	1.00	1.00	1.02	1.00	1.00	1.22	1.03	1.00
12/128	390	1.00	1.00	1.00	1.01	1.00	1.00	1.22	1.03	1.00
14/128	404	1.00	1.00	1.00	1.01	1.00	1.00	1.08	1.01	1.00

[a] Assuming a cost of 1 for gradients and energy calculations, 7 for a Hessian calculation, and 50 for stationary-point optimizations and frequencies.

TABLE 17: Ratio $k^{\text{IVTST-M-}H/G}/k^{\text{IVTST-M-28/254}}$ for the 1,5-Hydrogen Shift in 1,2-Pentadiene, As Described by the PM3 Surface[a]

		VTST			VTST/ZCT			VTST/SCT		
H/G	cost[b]	400 K	600 K	2400 K	400 K	600 K	2400 K	400 K	600 K	2400 K
2/20	104	1.00	1.00	0.93	0.20	0.60	0.91	0.12	0.54	0.90
2/38	140	1.00	1.00	1.00	0.40	0.79	0.99	0.26	0.75	0.99
4/38	154	1.00	1.00	1.00	0.51	0.87	1.00	0.34	0.82	0.99
4/56	190	1.00	1.00	1.00	0.70	0.95	1.00	0.49	0.91	1.00
6/56	204	1.00	1.00	1.00	0.79	0.97	1.00	0.58	0.95	1.00
6/74	240	1.00	1.00	1.00	0.91	0.99	1.00	0.70	0.97	1.00
8/74	254	1.00	1.00	1.00	0.96	1.00	1.00	0.80	0.99	1.00
8/92	290	1.00	1.00	1.00	1.00	1.00	1.00	0.85	0.99	1.00
10/92	304	1.00	1.00	1.00	1.02	1.00	1.00	0.95	0.99	1.00
10/110	340	1.00	1.00	1.00	1.03	1.00	1.00	0.96	1.00	1.00
12/110	354	1.00	1.00	1.00	1.02	1.00	1.00	1.02	1.00	1.00
14/146	440	1.00	1.00	1.00	1.01	1.00	1.00	1.03	1.00	1.00
16/146	454	1.00	1.00	1.00	1.00	1.00	1.00	1.03	1.00	1.00
20/200	590	1.00	1.00	1.00	1.00	1.00	1.00	1.01	1.00	1.00
22/200	604	1.00	1.00	1.00	1.00	1.00	1.00	1.00	1.00	1.00

[a] VTST denoted ICVT for $G = 20$ and CVT for $G > 20$ (see section 4). [b] Assuming a cost of 1 for gradients and energy calculations, 7 for a Hessian calculation, and 50 for stationary-point optimizations and frequencies.

Table 17, shows the ratio between interpolated and converged rate constants. Convergence is very smooth and reasonable for $H/G = 4/38$ or better at 400 K and 4/56 or better at 600 K.

5.11. $HBr + C_2H_2 \rightarrow CH_2CHBr$ Reaction, AM1 Surface. The last test is the addition reaction of HBr to C_2H_2, as described by the AM1 surface. For this calculation we used a reduced mass of 26 amu. The reason is that the addition of HBr to C_2H_2 involves a motion of the lighter C_2H_2 approaching to the heavier HBr, that can be seen as fixed. Therefore, a physically

TABLE 18: Ratio $k^{IVTST-M-H/G}/k^{IVTST-M-22/200}$ for the HBr + $C_2H_2 \rightarrow H_2CCHBr$ Reaction, As Described by the AM1 Surface

		CVT			CVT/ZCT			CVT/SCT		
H/*G*	cost[a]	400 K	600 K	2400 K	400 K	600 K	2400 K	400 K	600 K	2400 K
2/20	104	1.00	1.00	1.01	0.21	0.76	1.00	0.08	0.68	1.00
2/38	140	1.00	1.00	1.01	0.77	0.97	1.00	0.33	0.90	1.00
4/38	154	0.99	1.00	1.00	0.83	0.98	1.00	0.39	0.90	1.00
4/56	190	0.99	1.00	1.00	1.04	1.00	1.00	0.51	0.93	1.00
6/56	204	1.00	1.00	1.00	1.06	1.00	1.00	0.79	1.00	1.00
6/74	240	1.00	1.00	1.00	1.05	1.00	1.00	0.77	1.00	1.00
8/74	254	1.00	1.00	1.00	1.04	1.00	1.00	0.87	0.97	1.00
8/92	290	1.00	1.00	1.00	1.03	1.00	1.00	0.85	0.97	1.00
10/92	304	1.00	1.00	1.00	1.03	1.00	1.00	1.10	1.00	1.00
10/110	340	1.00	1.00	1.00	1.03	1.00	1.00	1.09	1.00	1.00
12/110	354	1.00	1.00	1.00	1.01	1.00	1.00	1.04	1.00	1.00
12/128	390	1.00	1.00	1.00	1.01	1.00	1.00	1.04	1.00	1.00
14/128	404	1.00	1.00	1.00	1.00	1.00	1.00	1.02	1.00	1.00
14/146	440	1.00	1.00	1.00	1.00	1.00	1.00	1.01	1.00	1.00
16/146	454	1.00	1.00	1.00	1.00	1.00	1.00	1.01	1.00	1.00

[a] Assuming a cost of 1 for gradients and energy calculations, 7 for a Hessian calculation, and 50 for stationary-point optimizations and frequencies.

realistic mass which to scale the reaction path is the mass of the C_2H_2 molecule.

For this reaction we again needed a step size of $0.003a_0$ in order to get an accurate reaction path. Therefore, we need about 3 times as much information as in previous tests for reaching the same distances along the reaction path.

For this reaction variational effects are once again negligible and tunneling is very important. Thus, according to the SCT method, the 400 K rate constant is increased by tunneling by a factor of about 650. The main problem in this test is obtaining a converged tunneling calculation for when such a high factor is present.

Table 18 shows the results for this reaction. For addition reactions, as in this test reaction, changes along the reaction path usually occur more gradually than for abstraction or transfer reactions. Consequently, the trends are easier to interpolate, and the rate constants are within a reasonable factor of the converged ones with little information. Nevertheless, the high tunneling factor for this reaction amplifies small differences between the interpolated and converged energies and frequencies. As a result, a calculation within 50% of the converged interpolated results requires at least a IVTST-M-4/56 calculation, which is roughly 20% of the information required for obtaining a converged rate constant without using IVTST-M.

5.12. Comparison of Cases. Table 19 compares the convergence rates of mapped calculations for each of the eight reactions. (See Table 3 for the convention used to label the cases.) In Table 19, as in Tables 4−18, each calculation is compared to calculations with the same gradient and Hessian step sizes and the same dynamical level (i.e., no tunneling, zero-curvature tunneling, or small-curvature tunneling), but in which the reaction path is followed in both the negative-*s* and positive-*s* direction until convergence is achieved with respect to the range covered. Thus this table is a direct test of the success of the mapping method for interpolating in the foothills, i.e., between the high-elevation regions near the barrier top and the reactant valley or plain one side and the product valley or plain on the other.

Table 19 shows that $H = 6$ is usually reasonably reliable as an indication of the fully converged results and $H = 9$ or 10 is systematically better, whereas $H = 4$ is somewhat more dangerous. We are quite pleased with the results. Consider,

TABLE 19: Unsigned Percentage Deviation from the Large-*H/G* Limit of Calculations with Much Smaller *H/G* at 300 K for Moderate-Barrier Reactions and at 600 K for High-Barrier Reactions[a]

case	H/G	VTST	VTST/ZCT	VTST/SCT
1	4/38	0[b]	30	41
2.1	4/38	0	100	71
3.2	4/38	0	6	26
4.2	3/56	84	217	144
5	4/38	0	10	2
6	4/38	0	34	24
7	4/38	0	13	18
8	4/38	0	2	10
av		10	49	42
1	6/56	0	21	37
2.3	6/56	0	1	26
3.2	6/56	0	1	14
4.2	6/56	0	32	48
5	6/56	0	7	5
6	6/56	0	13	43
7	6/56	0	3	5
8	6/56	0	0	0
av		0	10	22
1	10/92	0	7	23
2.3	9/83	0	14	13
3.2	10/92	0	1	3
4.2	9/83	0	8	10
5	10/92	0	3	3
6	10/92	0	1	8
7	10/92	0	0	1
8	10/92	0	0	0
av		0	4	7

[a] VTST denotes either ICVT or CVT as explained in section 4. [b] 0 denotes less than 0.5.

for example, the $CH_3 + H_2$ reaction. The present results show reasonable accuracy with $H = 4-6$, whereas our first calculations on this system[49] employed $H = 14$, and a more recent revisitation[50,51] of this reaction employed, depending on the level of the calculation, $H = 20$ or $H = 30$. Similarly, recent calculations on the $OH + H_2$ reaction employed $H = 24$ for a thermal calculation[52] while our calculations are reasonably accurate using $H = 4-6$. As another example we note that a recent calculation[53] on the $OH + H_2$ reaction employed $H = 334$ and $G = 16\,700$, although the goal of that paper was convergence to three significant figures, which is not our goal here.

6. Bottom Line Analysis

In section 5 we concentrated on the convergence of the calculation with respect to extending the reaction path farther from the saddle point and increasing the number of Hessians with a fixed interval between Hessians. We concentrated on that aspect because it provides the clearest indication of the adequacy and reliability of the mapped interpolation algorithm. The step sizes for those tests were chosen as realistic ones for practical applications, that is, small enough to prevent oscillations in reaction-path properties or secular wandering away from the true path, but not so small as to waste computer time by converging the calculations better than, say, 15% with respect to step sizes—such convergence would be unwarranted and unbalanced in light of the uncertainties in any practical electronic structure method.

However, as mentioned in section 5.1, we have also compared the IVTST-M calculations with these practical step sizes to fully converged CVT/SCT and ICVT/SCT calculations in which the calculations are converged with respect to the gradient and Hessian step sizes as well as the number of gradients and

TABLE 20: Ratios of Less-Expensive Rate Constants to Fully Converged VTST/SCT Calculations for Moderate-Barrier Cases

case	dynamical level	relative cost[a]	250 K	300 K	2400 K
1	TST	1.0	0.29	0.46	0.98
	ICVT/SCT−6/56	5.4	1.42	1.34	0.98
2.3	TST	1.0	5×10^{-4}	8×10^{-3}	0.96
	CVT/SCT−6/56	6.1	0.28	0.53	0.97
3.2	TST	1.0	0.12	0.28	1.17
	CVT/SCT−6/56	6.4	0.65	0.79	1.00
4.2	TST	1.0	0.03	0.13	4.30
	CVT/SCT−6/56	5.4	1.03	1.17	1.00
5	TST	1.0	0.68	0.78	1.04
	ICVT/SCT−6/56	6.8	0.88	0.93	0.88

[a] Relative to conventional transition-state theory.

TABLE 21: Ratios of TST and CVT/SCT-*H/G* Rate Constants to Fully Converged VTST/SCT Calculations for High-Barrier Cases

case	dynamical level	relative cost[a]	400 K	600 K	2400 K
6	TST	1.0	4×10^{-3}	0.10	0.88
	2/20	2.8	0.49	0.77	0.97
	4/38	4.1	0.91	1.08	0.98
	6/56	5.4	1.77	1.26	0.98
	8/74	6.8	1.47	1.06	0.98
7	TST	1.0	0.06	0.38	0.95
	2/20	2.8	0.13	0.56	0.90
	4/38	4.1	0.37	0.85	1.00
	6/56	5.4	0.63	0.97	1.00
	8/74	6.8	0.92	1.02	1.00
8	TST	1.0	2×10^{-3}	0.15	1.03
	2/20	2.8	0.08	0.68	1.00
	4/38	4.1	0.40	0.90	1.00
	6/56	5.4	0.81	1.00	1.00
	8/74	6.8	0.90	0.97	1.00

[a] Relative to conventional transition-state theory.

Hessians calculated. A full set of such comparisons are given in the Supporting Information, and in Tables 20 and 21 we present some highlights. This is the bottom line: how much computational effort is required to get an answer close to a fully converged CVT/SCT or ICVT/SCT calculation?

In Tables 20 and 21 we continue to use eq 20 for the nominal computational cost of a calculation. We emphasize again that eq 20 is very crude (as any such generic formula must be), but at least it allows a consistent way to estimate costs of various computational efforts.

Consider first the results at 250 K. Table 20 shows that conventional transition-state theory underestimated our best estimate by an order of magnitude (or more) in three out of five cases and by factors of 3.4 and 1.5 in the others. However, these errors are greatly reduced in all cases with $H = 6$, with an average percentage deviation from the fully converged results of only 30%. The results are equally impressive at 300 K, where the average percentage deviation is only 23%.

From Table 21, we see that IVTST-M yields remarkable improvement for the three high-barrier reactions too. At 400 K, conventional TST underestimates our best result by $1-2^1/_2$ orders of magnitude, whereas $H = 6$ gives an average error of only 44%. At 600 K, conventional TST underestimates our best result by an average factor of 6.4, which is reduced to an average factor of 1.5 with $H = 2$.

We could probably do better on individual reactions with further optimization of the interpolation parameters, but that was not our goal. Thus all results obtained here are obtained with "standard" parameters, and gradient and Hessian step sizes, typically $0.01a_0$ and $0.09a_0$ respectively, were not fine-tuned.

Another point worth emphasizing is that the present IVTST-M algorithm is not iterative, as the original IVTST-1 algorithm was.[11] Thus, in some cases the IVTST-1 algorithm encounters convergence problems, whereas this difficulty is not an issue with the present algorithm.

Finally we note that for all calculations in the present paper the frequencies were simply ordered by decreasing magnitude. Although better results can surely be obtained for specific cases by permuting frequencies to achieve diabatic crossings,[11,54] such permutations require system-specific intelligence, whereas our goal here is the development of a robust, automatic method.

7. Conclusion

We have presented a set of IVTST-M methods applicable to bimolecular and unimolecular reactions with a saddle point, based on the information about the stationary points along the reaction path plus G nonstationary points, with $G \geq 2$. The results are systematically improved by adding more data along the reaction path. We have developed a robust set of functional forms such that a single interpolation scheme with a fixed ratio of 9 between the Hessian and gradient step sizes performs well on a diverse collection of test cases. We make recommendations for all choices involved in the calculations so that future applications do not have to reoptimize them on a case-by-case basis.

The method proposed has been tested by calculating the rate constants for eight reactions, including both bimolecular and unimolecular reactions. In some cases we used information about a well along the reaction path for the interpolation. Sample percentage deviations from converged calculations are shown in Tables 19−21. All the results with $H \geq 6$ are quite reasonable, allowing calculations with useful accuracy based on a reduced amount of information along the reaction path. This method will allow dynamicists to focus our computational efforts on obtaining accurate electronic structure results for a small number of points along the reaction path instead of calculating a larger range of the reaction path at a lower level.

The tests show that usually (but not always) the calculation of Hessians along the entire available portion of reaction path is more efficient than extending the reaction path to cover a wider range without extending the range of the Hessian grid. They also show that including the properties of shallow wells along the reaction path does not always lead to a significant reduction in the computational effort needed for getting a converged rate constant. Since wells are usually very loose and hard to optimize, it seems in general more efficient to enlarge the range of the reaction path rather than locating the wells and calculating their properties. Nevertheless, in cases where the depth and location of the well seriously affect the shape of the $V_{MEP}(s)$ curve, extra computational effort for calculating the properties of the wells can be worthwhile.

The conjunction of these interpolation methods with other new ideas, such as dual-level methods[14,35] and VTST calculations without a minimum-energy path,[23] will provide even more promising tools for applying VTST to large systems, for which the usual method based on the calculation of the complete reaction path at the highest electronic level considered is unnecessarily expensive and often prohibitive.

Acknowledgment. J.C.C. acknowledges the Spanish Ministerio de Educación y Cultura and the Fulbright Commission for a postdoctoral scholarship. This work was also supported in part by the U.S. Department of Energy, Office of Basic Energy Sciences.

Supporting Information Available: Fully converged rate constants for all the eight reactions, longer versions of Tables 5 and 7, and analogues of Tables 4 to 19 in which the IVTST-M results are compared to fully CVT/SCT (or ICVT/SCT) converged results (22 pages). Ordering information is given on any current masthead page.

References and Notes

(1) Garrett, B. C.; Truhlar, D. G.; Grev, R. S.; Magnuson, A. W. *J. Phys. Chem.* **1980**, *84*, 1730; Erratum: **1983**, *87*, 4554.
(2) Isaacson A. D.; Truhlar, D. G. *J. Chem. Phys.* **1982**, *76*, 1380.
(3) Truhlar, D. G.; Isaacson, A. D.; Garrett, B. C. In *Theory of Chemical Reaction Dynamics*; Baer, M., Ed.; (CRC Press: Boca Raton, FL, 1985; Vol. 4, pp 65−137.
(4) Truhlar, D. G.; Garrett, B. C. *Annu. Rev. Phys. Chem.* **1984**, *35*, 159.
(5) Lu, D.-h.; Truong, T. N.; Melissas, V.; Lynch, G. C.; Liu, Y.-P.; Garrett, B. C.; Steckler, R.; Isaacson, A. D.; Rai, S. N.; Hancock, G. C.; Lauderdale, J. G.; Joseph, T.; Truhlar, D. G. *Comput. Phys. Commun.* **1992**, *71*, 235.
(6) Liu, Y.-P.; Lynch, G. C.; Truong, T. N.; Lu, D.-h.; Truhlar, D. G.; Garrett, B. C. *J. Am. Chem. Phys.* **1993**, *115*, 2408.
(7) Liu, Y.-P.; Lu, D.-h.; González-Lafont, A.; Truhlar, D. G.; Garrett, B. C. *J. Am. Chem. Soc.* **1993**, *115*, 7806.
(8) Jackels, C. F.; Gu, Z.; Truhlar, D. G. *J. Chem. Phys.* **1995**, *102*, 3188.
(9) Truhlar, D. G.; Gordon, M. S. *Science* **1990**, *249*, 491.
(10) Garrett, B. C.; Koszykowski, M. L.; Melius, C. F. In *Theoretical and Computational Models in Organic Chemistry*; Formosinho, S. J., Csizmadia, I. G., Arnaut, L. G., Eds.; Kluwer: Dordrecht, 1991; p 35.
(11) González-Lafont, A.; Truong, T. N.; Truhlar, D. G. *J. Chem. Phys.* **1991**, *95*, 8875.
(12) Truong, T. M.; Lu, D.-h.; Lynch, G. C.; Liu, Y.-P.; Melissas, V. S.; Stewart, J. J. P.; Steckler, R.; Garrett, B. C.; Isaacson, A. D.; González-Lafont, A.; Rai, S. N.; Hancock, G. C.; Joseph, T.; Truhlar, D. G. *Comput. Phys. Commun.* **1993**, *75*, 143.
(13) Page, M. *Computer Phys. Commun.* **1994**, *84*, 115.
(14) Hu, W.-P.; Liu, Y.-P.; Truhlar, D. G. *J. Chem. Soc., Faraday Trans.* **1994**, *90*, 1715.
(15) Truhlar, D. G. In *The Reaction Path in Chemistry: Current Approaches and Perspectives*; Heidrich, D., Ed.; Kluwer: Dordrecht, 1995; pp 229−255.
(16) Isaacson, A. D. In *The Reaction Path in Chemistry: Current Approaches and Perspectives*; Heidrich, D., Ed.; Kluwer: Dordrecht, 1995; pp 191−228.
(17) Truong, T. N.; Duncan, W. T.; Bell, R. L. *ACS Symp. Ser.* **1996**, *256*, 348.
(18) Steckler, R.; Thurman, G. M.; Watts, J.; Bartlett, R. J. *J. Chem. Phys.* **1997**, *106*, 3926.
(19) Chuang, Y.-Y.; Truhlar, D. G. *J. Phys. Chem. A* **1997**, *101*, 3808.
(20) Truhlar, D. G.; Kuppermann, A. *J. Am. Chem. Soc.* **1971**, *93*, 1840.
(21) Allison, T. C.; Truhlar, D. G. In *Modern Methods for Multidimensional Dynamics Computations in Chemistry*; Thompson, D. L., Ed.; World Scientific: Singapore, in press.
(22) Simons, J.; Nichols, J. *Quantum Mechanics in Chemistry*; Oxford University Press: New York, 1997; pp 444ff.
(23) Villà, J.; Truhlar, D. G. *Theor. Chem. Acc.* **1997**, *97*, 317.
(24) Marcus, R. A. *J. Chem. Phys.* **1966**, *45*, 4493.
(25) Fukui, K. In *The World of Quantum Chemistry*; Daudel, R., Pullman, A., Eds.; Reidel: Dordrecht, 1974; p 113.
(26) Melissas, V. S.; Truhlar, D. G.; Garrett, B. C. *J. Chem. Phys.* **1992**, *96*, 5758.
(27) Melissas, V. S.; Truhlar, D. G. *J. Chem. Phys.* **1993**, *99*, 1013.
(28) Corchado, J. C.; Espinosa-García, J.; Hu, W.-P.; Rossi, I.; Truhlar, D. G. *J. Phys. Chem* **1995**, *99*, 687.
(29) Renka, R. J. *SIAM J. Stat. Comput.* **1987**, *8*, 393.
(30) Renka, R. J. *ACM Trans. Math. Software* **1993**, *19*, 81.
(31) Chuang, Y.-Y.; Truhlar, D. G. *J. Phys. Chem.* **1998**, *102*, 242.
(32) Miller, W. H.; Handy, N. C.; Adams, J. E. *J. Chem. Phys.* **1980**, *72*, 99.
(33) POLYRATE-version 7.4; Steckler, R.; Chuang, Y.-Y.; Fast, P. L.; Coitiño, E. L.; Corchado, J. C.; Hu, W.-P.; Liu, Y.-P.; Lynch, G. C.; Nguyen, K. A.; Jackels, C. F.; Gu, M. Z.; Rossi, I.; Clayton, S.; Melissas, V. S.; Garrett, B. C.; Isaacson, A. D.; Truhlar, D. G. University of Minnesota, Minneapolis, 1997. See http://comp.chem.umn.edu/polyrate.
(34) Nguyen, K. A.; Jackels, C. F.; Truhlar, D. G. *J. Chem. Phys.* **1996**, *104*, 6491.
(35) Chuang, Y.-Y.; Truhlar, D. G. *J. Chem. Phys.* **1997**, *107*, 83.
(36) Chen, Z. *Theor. Chim. Acta* **1992**, *75*, 481.
(37) Schatz, G. C.; Elgersma, H. *Chem. Phys. Lett.*. **1980**, *73*, 21.
(38) GAUSSRATE-version 7.4; Corchado, J. C.; Coitiño, E. L.; Chuang, Y.-Y.; Truhlar, D. G. University of Minnesota, Minneapolis, 1997. See http://comp.chem.umn.edu/gaussrate.
(39) GAUSSIAN 94; Frisch, M. J.; Trucks, G. W.; Schlegel, H. B.; Gill, P. M. W.; Johnson, B. G.; Robb, M. A.; Cheeseman, J. R.; Keith, T.; Petersson, G. A.; Montgomery, J. A.; Raghavachari, K.; Al-Laham, M. A.; Zakrzewski, V. G.; Ortiz, J. V.; Foresman, J. B.; Cioslowski, J.; Stefanov, B. B.; Nanayakkara, A.; Challacombe, M.; Peng, C. Y.; Ayala, P. Y.; Chen, W.; Wong, M. W.; Andres, J. L.; Replogle, E. S.; Gomperts, R.; Martin, R. L.; Fox, D. J.; Binkley, J. S.; Defrees, D. J.; Baker, J.; Stewart, J. P. P.; Head-Gordon, M.; Gonzalez, C.; Pople, J. A. Gaussian Inc.: Pittsburgh, 1995.
(40) Joseph, T.; Steckler, R.; Truhlar, D. G. *J. Chem. Phys.* **1987**, *87*, 7036.
(41) Walch, S. P.; Dunning, T. H. *J. Chem. Phys.* **1980**, *72*, 72.
(42) Tucker, S. C.; Truhlar, D. G. *J. Phys. Chem.* **1989**, *93*, 8138.
(43) Dewar, M. J. S.; Zoebisch, E. G.; Healy, E. F. *J. Am. Chem. Soc.* **1985**, *107*, 3902.
(44) Stewart, J. J. P. *J. Comput. Chem.* **1989**, *10*, 221.
(45) Roothaan, C. C. J. *Rev. Mod. Phys.* **1951**, *23*, 69. Pople, J. A.; Nesbet, R. K. *J. Chem. Phys.* **1959**, *22*, 571.
(46) Møller, C.; Plesset, M. S. *Phys. Rev.* **1934**, *46*, 618.
(47) Hehre, W. J.; Stewart, R. F.; Pople, J. A. *J. Chem. Phys.* **1969**, *51*, 2657.
(48) Binkley, J. S.; Pople, J. A.; Hehre, W. J. *J. Am. Chem. Soc.* **1980**, *102*, 939.
(49) Baldridge, K. K.; Gordon, M. S.; Steckler, R.; Truhlar, D. G. *J. Phys. Chem.* **1989**, *93*, 5107.
(50) Truong, T. N. *J. Chem. Phys.* **1994**, *100*, 8014.
(51) Truong, T. N.; Duncan, W. T. *J. Chem. Phys.* **1994**, *101*, 7408.
(52) Truong, T. N.; Evans, T. J. *J. Phys. Chem.* **1994**, *98*, 9558.
(53) Isaacson, A. D. *J. Chem. Phys.* **1997**, *107*, 3832.
(54) Villà, J.; González-Lafont, A.; Lluch, J. M.; Bertrán, J. *Mol. Phys.* **1996**, *89*, 633.